STRESS ANALYSIS FOR TRUCK CHASSIS WITH RIVETED JOINTS

A Thesis Submitted to the
Graduate School of Natural and Applied Sciences of
Dokuz Eylül University
In Partial Fulfillment of the Requirements for
the Doctor of Philosophy in Mechanical Engineering,
Design and Production Program

by
Çiçek KARAOĞLU

June, 1998
İZMİR

Ph.D. THESIS EXAMINATION RESULT FORM

We certify that we have read this thesis and that in our opinion it is fully adequate, in scope and in quality. As a thesis for the degree of Doctor of Philosophy.

Prof. Dr. N. Sefa KURALAY

(Advisor)

Prof.Dr. Mustafa SAVCI

(Committee Member)

Y.Doç.Dr. Melih BELEVİ

(Committee Member)

Approved for the

Graduate School of Natural and Applied Sciences

Prof.Dr Cahit Helvacı

Director

Graduate School of Natural and Applied Sciences

ABSTRACT

The fact that most of the transportation is carried out on highways in our country , increases the importance of truck-type vehicles. Heavy loads and unstable road conditions may cause some structural problems on these vehicles after a certain service life. Typical problems are some time dependent failures caused by the increase in stress in some critical locations. Therefore, it is important to investigate the stress and strain values of chassis connections, which might lead to the solution of problems by design development.

In this study stress analyses of a truck chassis with riveted joints has been investigated. Nowadays, computer programs using finite elements are utilized for static and dynamic analysis of complex structures. In the method, a mathematical model of the structure is described. The model which has the static and dynamic properties of a real structure, is divided into finite elements of known elastic properties, and written in matrix form.

Developing computer technology and software are the tools for the solution of the problem. ANSYS. A general purpose finite element program has been used in this study. First of all, stress analysis of a general model of the chassis has been made. Results of this stage were rough due to the great dimensions of the model. Submodeling technique was utilized for more accurate results. The results of the first solution were used as the boundary conditions for the detailed models of the connections.

In the first stage of this study, stress distributions of two different chassis models. one of which has a fixed spring hanger(model 1). While other has movable (model 2), have been analyzed under three different road conditions.

Under the normal road conditions (road case 1), the stress values of the two different type of chassis have been found to be similar. But in the chassis model which has a fixed spring hanger(model 1), maximum principal stresses across the flange of the beam increases sharply. In the case of one rear wheel is free(road case2), which may occur the wheel drops into a hollow, the absolute stress values of the chassis with movable spring hanger(model 2) are found to be smaller than the other types values. In the case of a front wheel is free (road case3) stress values of the two types of connections increase. In the second stage of the study, the chassis with movable spring hanger (model2) which has lower stress values has been considered. And the effects of some modifications in connection plate have been investigated for the two road cases. Results can be summarized as follows:

Stress distribution of connection plates with various thickness as 6mm, 8mm, and 10mm has been analyzed. Maximum principal stresses decrease with increasing plate thickness .

The connection plate width has been changed (l=390, 430 and 470mm). Increasing plate width slightly decreases stress values under normal road conditions (road case1), while it increases stress values in the case of a fee front wheel (road case3). The increase in connection plate width decreases the flexibility of the connection which leads to an increase in stress and formation of tree axial stresses.

The main profile thickness of the chassis increased from 8mm to 13 mm, while the connection plate thickness decreased from 6 mm to 5 mm. Maximum principal stress decreases with increasing moment of inertia. But chassis weight increase %8.

It has been observed that any change of rivet distribution, rivet diameter and shape of connection plate also effects the maximum principal stress distribution.

Choosing a convenient rivet placement and optimizing connection width and thickness seem to be practical solutions for decreasing the stress values when a modification in the main profile of the chassis is not possible.

ÖZET

Ülkemizde, taşımacılığın çoğunun halen karayolu ile yapılması, kamyon tipi taşıtların önemini arttırmaktadır. Ağır yükler ve düzensiz yol şartlarında çalışan bu taşıtlarda belirli bir işletme süresi sonunda yapısal problemlerin ortaya çıkması olağandır. Ortaya çıkan problemler genellikle kritik bölgelerdeki gerilme artışı ve bunların zamanla neden olabileceği hasarlardır. Bu durumda şasi bağlantılarındaki daki gerilme ve deformasyon değerlerinin araştırılması, ortaya çıkabilecek sorunların yeni tasarımlarla giderilmesi açısından önemlidir.

Bu çalışmada perçinli kamyon şasi bağlantılarının gerilme analizi yapılmıştır. Günümüzde,kompleks yapıların statik ve dinamik analizleri, bugün sonlu elemanlar olarak bilinen yöntemler ile yapılmaktadır. Bu yöntemde yapı matematiksel olarak tasarlanır. Gerçek yapının statik ve dinamik özelliklerini içeren model bilinen elastik özelliklere sahip sonlu elemanlara bölünür ve matris formunda yazılır. Gelişen bilgisayar teknolojisi ve yazılımlar problemin çözülmesinde kullanılan araçlardır. Buradaki problemin çözümünde ANSYS (Analiz-Sistem) genel amaçlı sonlu eleman programı kullanılmıştır. İlk olarak genel hatları ile modellenen şasinin çeşitli yol konumları için çözümleri yapılmıştır. Modelin büyük olması nedeni ile elde edilen sonuçlar kabadır. Daha hassas sonuçlar elde edebilmek için alt modelleme (submodeling) tekniği kullanılmıştır. Bağlantılar ayrıca detaylı olarak modellenmiş ve ilk çözümden elde edilen sonuçlar bu bölüm için sınır şartı olmuştur.

İlk aşamada; şasi arka makas bağlantısının sabit (1.model) ve hareketli(2.model) olan iki farklı şasi modelinde üç farklı yol durumunda gerilme analizleri yapılmıştır. Düz yol konumunda (1.yol durumu) her iki şasi tipinde, bağlantılarda meydana gelen gerilme değerleri birbirine yakın çıkmıştır. Fakat arka makas bağlantısı sabit olan tipte

(1.model) ana profildeki enine kesit boyunca gerilmeler ani bir artış göstermektedir. Arka tekerleklerden birinin çukura düşmesi durumunda(2.yol durumu) arka makas bağlantısı hareketli olan tipte (2.model) meydana gelen gerilmeler mutlak değerce daha küçük çıkmaktadır. Bunun nedeni hareketli olan bağlantının kendini yol konumuna göre ayarlayarak bir mesnetteki fazla tepkiyi diğerine dengeli olarak dağıtmasından dolayıdır. Ön tekerin çukurda olması durumunda ise (3.yol durumu) her iki tiptede ara makas bağlantısındaki gerilme değerleri artmıştır.

İkinci aşamada farklı yol konumlarına daha küçük gerilmelerin meydana geldiği arka makas bağlantısı hareketli olan şasi tipi (2.model) ele alınarak, bağlantıdaki değişikliklerin gerilmeleri düz yolda ve ön tekerin çukurda olması durumunda nasıl etkilediği araştırılmıştır.

Bağlantı plakası kalınlığı (t) 6mm, 8mm ve 10mm lik değerleri,için gerilme dağılımları incelenmiştir. Kalınlığın artması ile bağlantı plakasındaki gerilmelerin azaldığı görülmüştür.

Bağlantı plakası genişliğinin (l) 390mm, 430mm ve 470mm gibi farklı değerleri için, gerilme dağılımları incelenmiştir. Bağlantı plakası genişliğindeki artış düzyol durumunda gerilmelerin azalmasına, ön tekerleğin çukurda olması durumunda ise, üç eksenli gerilmelerin doğmasına ve gerilmelerin artmasına neden olmuştur.

Şasi ana profil kalınlığı 8mm' den 13 mm'ye çıkartılıp bağlantı plakası kalınlığı 6mm'den 5 mm' ye azaltıldığı başka incelemede: kalınlığın artması ile atalet momentinin artması sonucunda gerilmelerde önemli bir azalma, buna karşın şaşi ağırlığında %8'lik bir artış meydana gelmiştir.

Bağlantı plakası şekli, perçin yerleri ve perçin çaplarında yapılan değişimlerin de gerilmeler üzerinde etkisi olduğu görülmüştür.

Şasi ana profilindeki değişimin mümkün olmadığı durumlarda, uygun perçin yerleşimi veya uygun bağlantı kalınlığı ve genişliği ile gerilmelerin azaltılması pratik bir çözüm olarak görülmektedir.

ACKNOWLEDGEMENTS

I am gratefully acknowledge the support and encouragement given by Prof.Dr. N. Sefa KURALAY during the course of the investigation. I wish to express my thanks to Prof.Dr. Onur SAYMAN for his kind support during the study. I wish to thank Prof. Dr. Tülay HARZADIN, the Head of Mechanical Engineering Department, for supplying the ANSYS program used in the present study. I am indebted to Prof.Dr. Mustafa DEMİRSOY and Dr. Atilay YEŞİL for supplying valuable documents. I am grateful toDr. Melih BELEVİ, and Hayri DOĞRU for their continuing support. I am also grateful to Hikmet GÜRBÜZ, Zeki KIRAL and Mehmet ZOR for their personal support. During the thesis, assistance from these friends is also appreciated: Zafer DİCLE, Savaş KOÇER, Serat KORSACILAR, Sefer KÜÇÜK and Kemal VAROL. I wish to express my gratitude for the financial support given by AFS and Technical support given by Rahmi AKIN and Muharrem ATÇELER from BMC. Finally,I thank my family and my husband for their great help, encouragement and patience that supported me throughout the study.

Çiçek KARAOĞLU

CONTENTS

Page

Page

LIST OF TABLES

LIST OF FIGURES

Page

Page

Page

Page

NOMENCLATURE

b : Chassis frame width

L : Chassis frame

L_1 : Active load length

E : Modulus of elasticity

G : Shear modulus of elasticity

ν : Poisson's ratio

$\{F\}^e$: Column vector of the nodal forces of the element e

$[K]^e$: Stiffness matrix of the element e

$\{U\}^e$: Nodal displacement vector of the element e

t : Thickness of element e

$\{F\}$: Column vector of the nodal forces of the entire system

$[K]$: Stiffness matrix of the entire system

$\{U\}$: Nodal displacement vector of the entire system

r,s : Natural Coordinate

x,y : Global Coordinate

$\{q\}$: Displacement vector

$[D]$: Elasticity matrix of material

$[B]$: Transformation matrix between strain and displacement

$\{\sigma\}$: Stress vector

$\{\varepsilon\}$:Strain vector

J : Jacobian operator

S_1,S_2,S_3 : Principal stresses

N_1,N_2,N_3,N_4 : Shape functions of quadrilateral element

CHAPTER ONE
INTRODUCTION

The static and dynamic analysis of complex structures can be accomplished by the use of currently available computer programs where they can be described by a fine mesh of finite elements. The results of such analyses should give an insight into the load distribution in the various members of the structure so that a desirable load distribution can be arrived at gradually in the process of design.

The grillages normally used as a chassis frame of commercial vehicle appears to be simple structures, which explains why they are frequently only analyzed by equally simple methods. However, accurate analysis of load-deformation characteristics especially the analysis of stress distributions are actually quite difficult.

The basic idea of a force method to analyze the whole frame, with an approximation for the effect of the joints the first paper was written in 1968 by vehicle structures groups. Several writers have explored the idea of using different finite element programs for analyzing the joints and the main framework.

Marshall et al and Megson and Alade applied the MFM for the overall analysis too. Both authors found that agreement with experimental results is achieved only if partial warping inhibition is included in the overall stiffness calculation. Megson gains warping restraint factors by finite element calculations of semi-cross-member and the associated side-member web, while the Marshall treats the side member web as a plate in bending. (Marshall,1968, Megson, Alade,1976)

A computer program was developed for the calculation of vehicle frame torsion by MFM. It allows for variable numbers of cross-members and out of plane shear center axes.(Oehlschlaeger,1977)

Warping inhibition in the joints of vehicle frames with open-cross section members was investigated by Beermann. Employing the compatibility condition of the rates of twist in the joints to determine the bimoments makes it necessary to take the flexibility of the joints into consideration.(Beermann,1977)

Beerman presents the vehicle frames with closed cross section cross-member under torsion.(Beerman 1977)

The flexibility matrix has to be calculated numerically by finite elements. Rate of twist flexibilities exceeding the range have only a small effect on the torsional stiffness and the bimoments of typical truck-frame. (Oehlschlaeger,1980).

Kwangju Lee presented a method of flexible joints in vehicle structures . The method identifies the most important parameters of a joint model and estimates their values by using displacement measurements of the overall structure (Lee,1992).

Influence of the nodal layout on the torsional rigidity and torsional stresses of torsionally flexible frames of commercial vehicles reported by the Oehlschlaeger. (Oehlschlaeger,1980)

East European researchers have also made use of an additional degree of freedom for the bi-moment and the associated displacement.(Tidbury,1980)

In 1984 Beermann presents a hybid method of analysis which combines finite element idealization of the joint areas with analytically derived beam elements for the cross member and a side member sections. The beam element includes warping torsion force displacement relationships. The flexibility of the joints is included together with the compatibility of their displacements. (Beermann,1984)

Numerical calculation based on the finite element method seems have become widely accepted as a helpful tool with in the design and development departments of the automotive industry. The reason for this is two fold: on the one hand user experience is growing, on the other hand the software capabilities for preprocessing , calculation and postprocessing have reached a certain state of convenience, allowing interactive handling and graphic presentation of results. There are various standard textbooks which provide detailed information, e.g. from an engineering point of view there is Zienkiewicz or more theoretically Oden.(Zienkiewicz,1997, Oden,1971).

In this study, stress analysis of commercial vehicle frames with riveted joints has been investigated by the finite element method. In the solution ANSYS program which is a general computer program for finite element analysis was used.

In the second chapter, the general finite element method procedures are defined. These are generation of the finite element meshes, the isoparametric elements, interpolation functions, obtaining the element properties, assembly of the element, solving the system equations and making additional computations.

Definition of the two dimensional isoparametric finite element and the formulation, calculations of its matrices and numerical integration are given in general form in the third chapter.

Information about truck chassis and loads act on a chassis frame are given in the fourth chapter.

In the fifth chapter, definition of the problem, finite element model, boundary conditions and material properties are presented.

Results and discussion are reviewed in chapter sixth chapter.

Conclusion are given in the eighth chapter.

In Appendix A submodeling technique are presented.

In Appendix B computer program is presented in detail.

CHAPTER TWO

FINITE ELEMENT METHOD

2.1 INTRODUCTION

In essence the finite element method is a numerical procedure for solving the ordinary and partial differential equations that arise in engineering and mathematical physics.

The method is applicable to problems in such diverse fields as frame analysis, stress analysis of solid continua, fluid dynamics, heat flow, and electrical field theory, to name a few. Its development has now reached the stage where it is the most commonly used method of numerical analysis.

In the early 1960's, engineers used the method for approximate solution of problems in stress analysis, fluid flow, heat transfer and other areas. A book by Argyris in 1955 on energy theorems and matrix methods laid a foundation for further developments in finite elements studies. The first book on finite elements by Zienkiewicz and Chung was published in 1967. In the late 1960's and early 1970's, finite element analysis was applied to nonlinear problems and large deformations. Mathematical foundations were laid in the 1970's. New element development, convergence studies, and other related areas fall in this category.

By the early 1970's package programs for finite element analysis become widely available and routine analysis of stresses and displacements in complex plate and shell structures or solid object was practicable.

Nowadays, complex problems can be modeled with relative ease, with the advances in computer technology and CAD systems. Several alternative configurations can be tried out on a computer before the first prototype is built. All of this suggests that we need to keep pace with these developments by understanding the basic theory, modeling techniques, and computational aspects of the finite element method.

In this method of analysis the structure is divided into simple geometric imaginary shapes called finite elements. The material properties and governing relationships are considered over these elements and expressed in terms of unknown values at element corners. An assembly process, duly considering the loading and constraints, results in a set of equations. Solution of these equations gives us the approximate behavior of the continuum.

Fiqure2.1 shows some of the element types available for finite element analysis. These are triangle element, quadrilateral element, axial symmetric triangle or quadratic element, tetrahedron element, hexahedral element, shell element etc.

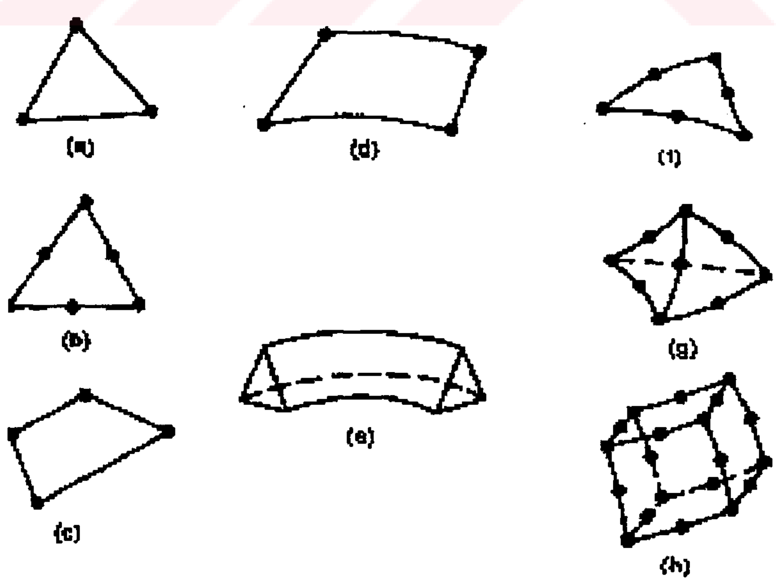

Figure 2.1. Some common elements used in the finite element method analysis.

A finite element analysis involves three stages of activity (Chandrupatla,1991)
Preprocessing, prosessing, and postprocessing

* Preprocessing involves preparation of data, such as nodal coordinates, connectivity, boundary conditions and loading and material information.
* The processing stage involves stiffness generation, stiffness modification and solution of equations, resulting in the evaluation of nodal variables.
* The postprocessing stage deals with the presentation of results. The deformed configuration, mode shapes, temperature, and stress distribution are computed and displayed at this stage.

The power of the finite element method resides principally in its versatility. The method can be applied to various physical problems. The body analyzed can have arbitrary shape, loads, and support conditions. The mesh can mix elements of different types, shapes and physical properties. This great versatility is contained within a single computer program. User prepared input data controls the selections of problem type, geometry, boundary condition, element selection, and so on.

The finite element method also has disadvantages. A specific numerical result is found for a specific problem. A finite element analysis provides no closed form solution that permits analytical study of effects of changing various parameters. A computer, a reliable program, and intelligent use are essential. A general purpose program has extensive documentation, which can not be ignored. Experience and good engineering judgment are needed in order to define a good model. Many input data are required and voluminous output must be stored and understood.

2.2 GENERATION OF FINITE ELEMENT MESH

The first step in a finite element analysis is to select the type of element and the corresponding finite element mesh. There are no fixed rules on how to make decisions. Clearly, for a given type of element the accuracy increases with decreasing element and, in general, one will use small elements in regions where the unknown function stress, say -varies rapidly. This means that a sound physical understanding of the problem considered is of fundamental importance for a realistic analysis. However, the decision on element types and size is more delicate then that. Every analysis involves the use resources, whether they are measured in terms of money or manpower, and even though we aim at an accurate analysis, we do not want it to be more accurate than required. For some problems, we are interest in detailed information on the behavior even in local regions, while for others we only want to obtain a rather general and crude indication of the overall response. As engineers we must therefore use our judgment in order to obtain that optimum choice for element type and element mesh which balances the requirement of reliable results with that of course effectiveness.

All finite elements are based on rather simple polynomial interpolations of the unknown function within the element. For a given type of element this means that smaller the elements, the greater the accuracy. However, it also implies that any dimension of an element should be kept as a small as possible, i.e..it is not only the size, but also the form of the element which is importance. As an example, assume that quadrilateral shown in Figure2.2 is divided into two triangular elements.

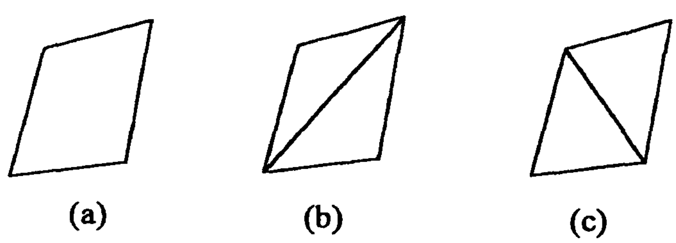

Figure2.2 a- Quadrilateral element b-inferior decision c- desirable division

It is obvious that the division in Figure 2.2c is better than 2.2.b, since largest dimension of the element Figure 2.2c is smaller than that give by 2.2b. The ratio between the largest and smallest dimension of an element is called aspect ratio and in a good finite element mesh, the aspect ratio is as close as possible to unity.

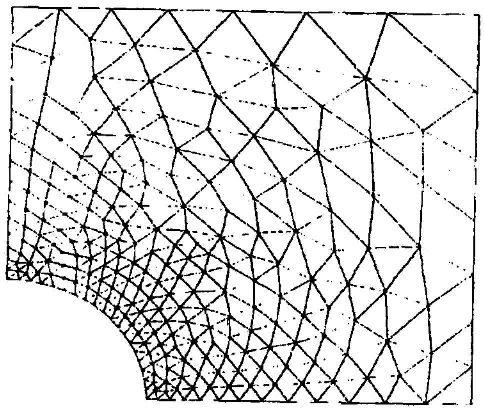

Figure2.3. Mesh refinement for the finite element analysis.

In order to obtain an efficient solution scheme, we want to use few elements in regions where unknown function varies slowly, but many elements in regions where it varies rapidly. Two possibilities, which allow for such a mesh refinement and which fulfill the continuity requirement are illustrated Figure 2.3. for the three node triangular element.

2.3 ISOPARAMETRIC ELEMENTS

Isoparametric elements are defined as elements for which the equations required to define the element shape are identical to those used to define the displacement fields with in the element. The advantage of isoparametric elements is that the displacement interpolations can be used directly to provide a mapping of elements of simple basic shape(such as rectangles and triangles) into more general shapes (such as quadrilaterals and triangles with curve sides) and thus whole new series of versatile elements is produced.

In formulating isoparametric elements, natural coordinate system must be used (systems r,s and r,s,t in Figure 2.4). Displacements are expressed in terms of natural coordinates, but must be differentiated with respect to global coordinates x,y,z. Some of the isoparametric elements are shown in Figure 2.4.

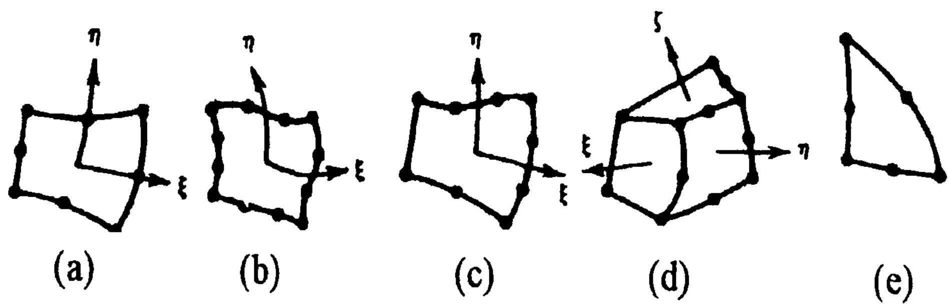

Figure 2.4. Some of the Isoparametric Elements. a-Quadratic plane element . b-Cubic plane element c-A degraded cubic element. d-Quadratic solid element with some linear edges. e-A quadratic plane triangle.

2.4. INTERPOLATION FUNCTIONS

Interpolation or shape functions represents the behavior of field variable with in an element.

Although it is conceivable that many types of functions could serve as interpolation functions, only polynomials have received widespread use. The reason is that polynomials are relatively easy to manipulate mathematically, in other words, they can be integrated or differentiated without difficulty.

2.4.1 NATURAL COORDINATES

A local coordinate system that relies on the element geometry for its definition and whose coordinate range between zero and unity within the element is known as a natural coordinate system.

The basic purpose of the natural coordinate system is to describe the location of a point inside an element in terms of coordinates associated with the nodes of the element. It will become evident that the natural coordinates are functions of the global cartesian coordinate system in which the element is defined.

A general quadrilateral element in the global cartesian coordinate system and local natural coordinate system are shown in Figure 2.5. In the natural coordinate system whose origin is at the center of the quadrilateral element is a square with sides extending $r=\pm1$, $s=\pm1$.

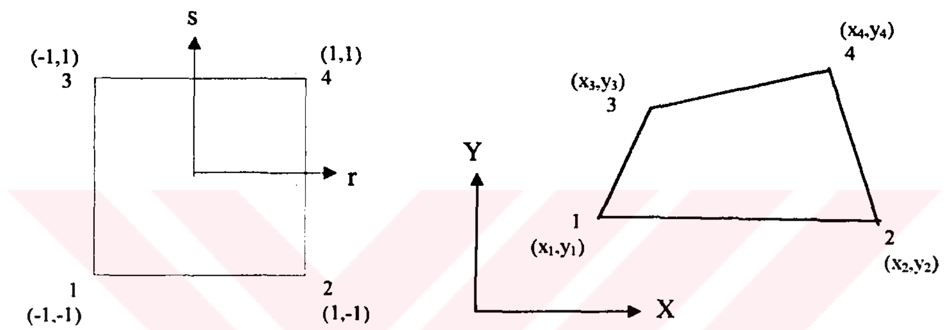

a). Natural coordinates b).global coordinates

Figure 2.5. Natural Coordinates for a general quadrilateral. a-Global cartesian coordinates. b- Natural coordinates.

2.5 OBTAINING THE ELEMENT PROPERTIES

Having at hand a suitable variational principle, the general finite element equation for elastic continuum are developed. The force-displacement equations for the element can be written as (Zienkiewicz,1982)

$$[K]^e\{u\}^e = \{F\}^e \tag{2.1}$$

where $[K]^e$ is the stiffness matrix of the element(e), $\{u\}$ is the nodal displacements vector, and $\{F\}^e$ is a column vector of the nodal forces of the element.

2.6 ASSEMBLY OF THE ELEMENT PROPERTIES

The complete force displacement equations for discretized solid are assembled from the sets of element equations like Eq.(2.1). The system equations have the same form as the element equations except that they are expanded in dimension to include all nodes. Hence when discretized system has n nodes, the system equations become

$$[K]\{U\} = \{F\} \tag{2.2}$$

where [K] is stiffness matrix, $\{U\}$ are the column vector of the nodal displacements for entire system, and $\{F\}$ are the column vector of resultant nodal forces.

2.7 SOLVING THE SYSTEM EQUATIONS

After the stiffness matrix[K] and the force vector $\{F\}$ are obtained and boundary conditions are inserted, the equations can be solved by using any of the standard methods solving linear simultaneous algebraic equations.

2.8 MAKING ADDITIONAL COMPUTATIONS

After the system equations are solved for the nodal displacement, the stress at any point in any of the element can be calculated as follows.

$$\{\sigma\}^e = [C^e][B^e]\{u\}^e \tag{2.3}$$

CHAPTER THREE
STIFFNESS MATRIX DERIVATION OF THE SHELL ELEMENT

3.1 INTRODUCTION

Calculation of the finite element matrices are very important phase of a finite element analysis. In most practical analysis, the use of isoparametric finite element is more effective.

The basic procedure is the isoparametric finite element formulation is to express the element coordinates and element displacements in the form of the interpolations using the natural coordinate system of the elements.

3.2 TWO DIMENSIONAL ISOPARAMETRIC ELEMENT

The general quadrilateral element is shown in Figure 3.1. The local nodes are numbered 1,2,3,4 a counterclokwise fashion as shown, and (x_i,y_i) are the coordinates of node I.

The vector

$$\{u\}=[u_1,v_1,u_2,v_2, \ldots,u_i,v_i]^T \tag{3.1}$$

denotes the element displacement vector. The displacement of an interior P at located at (x,y) is represented as

$$u=[u(x,y),v(x,y)]^T \tag{3.2}$$

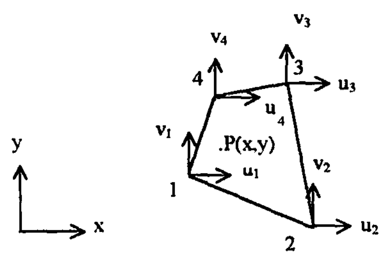

Figure3.1 Four node quadrilateral element

3.3 SHAPE FUNCTIONS

The master element shown in Figure 3.2. is defined r, s coordinates (or natural coordinates) and is square shaped. The shape functions N_i where i=1,2,3,4 are defined such that N_i is equal to unity at node i and is zero at other nodes.

In particular, consider the definition of N_i ; $N_1=1$ at node 1; $N_1=0$ at node 2,3,4

The requirement that $N_1=0$ at nodes 2,3 and 4 is equivalent to requiring that $N_1=0$ along edges r=+1 and s=+1. Thus N_1 has to be of the form

$$N_1 = c(1-r)(1-s) \tag{3.3}$$

where c is a constant. The constant is determined from the condition $N_1=1$ at node 1, since r = -1, s= -1 at node 1,

$$1=c(2)(2) \tag{3.4}$$

Thus c is obtained as 1/4

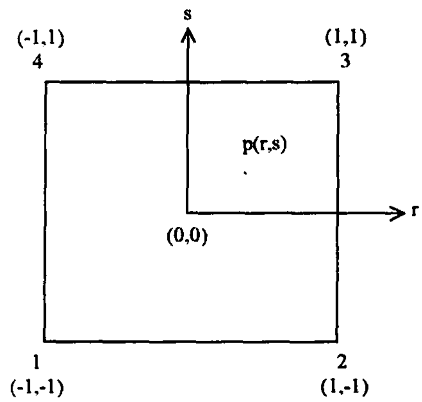

Figure 3.2. Four node quadrilateral element natural r,s coordinates

$$\begin{aligned} N_1 &= \frac{1}{4}(1-r)(1-s) \\ N_2 &= \frac{1}{4}(1+r)(1-s) \\ N_3 &= \frac{1}{4}(1+r)(1+s) \\ N_4 &= \frac{1}{4}(1-r)(1+s) \end{aligned} \tag{3.5}$$

If $u=[u,v]^T$ represents the displacement components of a point located as (r,s) and {u} is the element displacement vector, then

$$u = \sum_{i=1}^{4} N_i u_i \quad , \quad v = \sum_{i=1}^{4} N_i v_i \tag{3.6}$$

$$\begin{aligned} u &= N_1 u_1 + N_2 u_2 + N_3 u_3 + N_4 u_4 \\ v &= N_1 v_1 + N_2 v_2 + N_3 v_3 + N_4 v_4 \end{aligned} \tag{3.7}$$

which can be written in matrix form as

$$u = N\{u\} \tag{3.8}$$

where

where

$$N = \begin{bmatrix} N_1 & 0 & N_2 & 0 & N_3 & 0 & N_4 & 0 \\ 0 & N_1 & 0 & N_2 & 0 & N_3 & 0 & N_4 \end{bmatrix} \tag{3.9}$$

In the isoparametric formulation, we use the same shape function N_i to also express the coordinates of a point with in the element in terms of nodal coordinates.

$$\begin{aligned} x &= N_1x_1 + N_2x_2 + N_3x_3 + N_4x_4 \\ y &= N_1y_1 + N_2y_2 + N_3y_3 + N_4y_4 \end{aligned} \tag{3.10}$$

Subsequently, we need to express the derivatives of a function in x,y coordinates in terms of its derivatives in r,s coordinates. This is done as follows. A function f=f(x,y), in view of Eqs.(3.10), can be considered to be an implicit function of r and s f=f[x(r,s),y (r,s)].

Using the chain rule of differentiation, we have

$$\begin{aligned} \frac{\partial f}{\partial r} &= \frac{\partial f}{\partial x}\frac{\partial x}{\partial r} + \frac{\partial f}{\partial y}\frac{\partial y}{\partial r} \\ \frac{\partial f}{\partial s} &= \frac{\partial f}{\partial x}\frac{\partial x}{\partial s} + \frac{\partial f}{\partial y}\frac{\partial y}{\partial s} \end{aligned} \tag{3.11}$$

or

$$\begin{Bmatrix} \dfrac{\partial f}{\partial r} \\ \dfrac{\partial f}{\partial s} \end{Bmatrix} = J \begin{Bmatrix} \dfrac{\partial f}{\partial x} \\ \dfrac{\partial f}{\partial y} \end{Bmatrix} \tag{3.12}$$

Where J is the Jacobean matrix

$$J=\begin{bmatrix}\frac{\partial x}{\partial r} & \frac{\partial y}{\partial r}\\ \frac{\partial x}{\partial s} & \frac{\partial y}{\partial s}\end{bmatrix} \tag{3.13}$$

In view of Eqs.3.4 and 3.12 , we have

$$J=\frac{1}{4}\begin{bmatrix}-(1-s)x_1+(1-s)x_2+(1+s)x_3-(1+s)x_4 & -(1-s)y_1+(1-s)y_2+(1+s)y_3-(1+s)y_4\\ -(1-r)x_1-(1+r)x_2+(1+r)x_3+(1-r)x_4 & -(1-r)y_1-(1+r)y_2+(1+r)y_3+(1-r)y_4\end{bmatrix}$$

$$=\begin{bmatrix}J_{11} & J_{12}\\ J_{21} & J_{22}\end{bmatrix} \tag{3.14}$$

Equation 3.9 can be inverted as

$$\begin{Bmatrix}\frac{\partial f}{\partial x}\\ \frac{\partial f}{\partial y}\end{Bmatrix}=J^{-1}\begin{Bmatrix}\frac{\partial f}{\partial r}\\ \frac{\partial f}{\partial s}\end{Bmatrix} \tag{3.15}$$

$$\begin{Bmatrix}\frac{\partial f}{\partial x}\\ \frac{\partial f}{\partial y}\end{Bmatrix}=\frac{1}{\det J}\begin{bmatrix}J_{22} & -J_{12}\\ -J_{21} & J_{11}\end{bmatrix}\begin{Bmatrix}\frac{\partial f}{\partial r}\\ \frac{\partial f}{\partial s}\end{Bmatrix} \tag{3.16}$$

These expressions will be used in the derivation of the element stiffness matrix. In additional result that will be needed is the relation

$$dxdy = \det J drds \tag{3.17}$$

3.4 DERIVATION ELEMENT STIFFNESS MATRIX

A simple rectangular flat shell element can be obtained by superimposing the plate bending behavior and the plane stress behavior of the element as shown in Figure3.3.

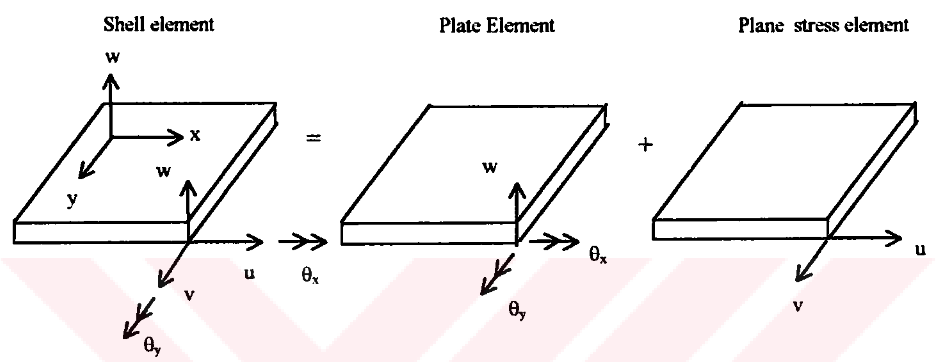

Figure3.3. Basic shell element with local 5 degrees of freedom at a node.

The displacement components of a point of coordinates x, y, z are in small displacement bending theory

$$u = z\theta_x(x,y) \qquad v = -z\theta_y(x,y) \qquad w = w(x,y) \tag{3.18}$$

Where w is the transverse displacement , θ_x and θ_y are the rotations of the normal to the undeformed middle surface.

The stiffness matrix for the flat shell element can be derived from the strain energy in the body given by

$$U = \int_v \frac{1}{2}\sigma^T \varepsilon dV + \int_v \frac{1}{2}\sigma^T \varepsilon dV + \tag{3.19}$$

The generalized strain vector ε can be defined as

$$\varepsilon(x,y)=\begin{Bmatrix} \dfrac{\partial u}{\partial x} \\ \dfrac{\partial v}{\partial y} \\ \dfrac{\partial u}{\partial y}+\dfrac{\partial v}{\partial x} \\ \dfrac{\partial \theta_x}{\partial y} \\ -\dfrac{\partial \theta_y}{\partial x} \\ -\dfrac{\partial \theta_y}{\partial y}+\dfrac{\partial \theta_x}{\partial x} \end{Bmatrix} \tag{3.20}$$

By considering f=u in Eq.3.16, we have

$$\begin{Bmatrix} \dfrac{\partial u}{\partial x} \\ \dfrac{\partial u}{\partial y} \end{Bmatrix}=\frac{1}{\det J}\begin{bmatrix} J_{22} & -J_{12} \\ -J_{21} & J_{11} \end{bmatrix}\begin{Bmatrix} \dfrac{\partial u}{\partial r} \\ \dfrac{\partial u}{\partial s} \end{Bmatrix} \tag{3.21}$$

Similarly

$$\begin{Bmatrix} \dfrac{\partial v}{\partial x} \\ \dfrac{\partial v}{\partial y} \end{Bmatrix}=\frac{1}{\det J}\begin{bmatrix} J_{22} & -J_{12} \\ -J_{21} & J_{11} \end{bmatrix}\begin{Bmatrix} \dfrac{\partial v}{\partial r} \\ \dfrac{\partial v}{\partial s} \end{Bmatrix} \tag{3.22}$$

we can write Equation 3.10 in the matrix form as

$$\varepsilon = Bu \tag{3.23}$$

where B the strain-displacement matrix is given by

$$B = \begin{bmatrix} b_1 & b_2 & . & . & b_n \end{bmatrix} \tag{3.24}$$

B is a matrix of 5x20.

$$b_i = \begin{bmatrix} \frac{\partial N_i}{\partial x} & 0 & 0 & 0 & 0 \\ 0 & \frac{\partial N_i}{\partial y} & 0 & 0 & 0 \\ \frac{\partial N_i}{\partial y} & \frac{\partial N_i}{\partial x} & 0 & 0 & 0 \\ 0 & 0 & 0 & \frac{\partial N_i}{\partial x} & 0 \\ 0 & 0 & 0 & 0 & -\frac{\partial N_i}{\partial y} \\ 0 & 0 & 0 & \frac{\partial N_i}{\partial y} & -\frac{\partial N_i}{\partial x} \end{bmatrix} \tag{3.25}$$

It is seen that the first three rows in b_i originate from the membrane part, the next three from the bending terms .

The stress is given by

$$\sigma = CBu \tag{3.26}$$

Where C is the elasticity matrix given by

$$C = \begin{bmatrix} 1 & -\nu & 0 & 0 & 0 & 0 \\ -\nu & 1 & 0 & 0 & 0 & 0 \\ 0 & 0 & 2(1+\nu) & 0 & 0 & 0 \\ 0 & 0 & 0 & \frac{Et^3}{12(1-\nu^2)} & \frac{\nu Et^3}{\nu 12(1-\nu^2)} & 0 \\ 0 & 0 & 0 & \frac{\nu Et^3}{12(1-\nu^2)} & \frac{Et^3}{12(1-\nu^2)} & 0 \\ 0 & 0 & 0 & 0 & 0 & \frac{(1-\nu)Et^3}{24(1-\nu^2)} \end{bmatrix} \tag{3.27}$$

The strain energy in Equation 3.19 becomes

$$U = \sum \frac{1}{2} u^T \left[t_e \int_{-1}^{1} \int_{-1}^{1} B^T C B \det J dr ds \right] \tag{3.28}$$

$$= \sum_e \frac{1}{2} u^T k^e u \tag{3.29}$$

where

$$k^e = t_e \int_{-1}^{1} \int_{-1}^{1} B^T C B \det J dr ds \tag{3.30}$$

is the element stiffness matrix .

3.5 ELEMENT FORCE VECTOR

Body Force . A Body force which is distributed force per unit volume, contributes to the global load vector F. This contribution can be determined by considering the the body force term in the potential energy expression

$$\int_V u^T f dV \tag{3.31}$$

Using u=N{u}, and treating the body force $f=[f_x, f_y]^T$ as constant within each element, we get

$$\int u^T f dV = \sum_e \{u\}^T f^e \tag{3.32}$$

where the element body force vector is given by

$$f^{e} = \left[t_e \int_{1}^{1} \int_{1}^{1} N^{T} \det J dr ds \right] \begin{Bmatrix} f_x \\ f_y \end{Bmatrix} \qquad (3.33)$$

Traction Force. Assume that a constant traction force, $T=[T_x,T_y]^T$, a force per unit area is applied on edge 2-3 of the quadrilateral element.. Along this edge, we have r=1. If we use the shape functions given in Equation(3.4) , this becomes $N_1=N_4=0$, $N_2=(1-s)/2$, $N_3=(1+r)/2$. Note that the shape functions are linear functions along the edges. Consequently, from the potential, the element traction load vector is readily given by

$$T^{e} = \frac{t_e l_{2-3}}{2} \begin{bmatrix} 0 & 0 & T_x & T_y & T_x & T_y & 0 & 0 \end{bmatrix}^{T} \qquad (3.34)$$

where l_{2-3}=length of edge 2-3. For varying distributed loads, we may express T_x and T_y in terms of values of nodes 2 and 3 using shape functions.

3.6 NUMERICAL INTEGRATION

The finite element matrices .can be solved by numerical integration. Consider the problem of numerically evaluating a one dimensional integral of the form

$$I = \int_{1}^{1} f(r)dr \qquad (3.35)$$

The gaussian guadrature approach is the most useful in finite element work. The gaussion quadrature approach are given below.

Consider the n-point approximation

$$I=\int_{-1}^{1} f(r)dr \approx w_1 f(r_1)+w_2 f(r_2)+............+w_n f(r_n) \qquad (3.36)$$

where $w_1,w_2,...,w_n$ are the **weights** and $r_1,r_2,.....,r_n$ are the **Gauss points**. The idea behind Gaussian Quadrature is to select the n Gauss points and n Weights such that Eq.(3.36) provides an exact answer for polynomials f(r) of as large a degree of possible.

CHAPTER FOUR

TRUCK CHASSIS FRAMES

4.1 INTRODUCTION

Every vehicle has a body which has to carry both the loads and its own weight. Vehicle body consist of two parts chassis and bodywork or superstructure.

Trucks have chassis frames as the intrinsic load-carrying framework. The structural behavior of the frame is also dependent on the structural characteristics of any superstructure attached to it.

The foundation of the truck chassis units are usually is a frame on which different chassis units are mounted, and to which the axles are attached by the springs, and sometimes also by other members serving to transmit or take up the axle thrust and torque reaction.

The conventional frame, which is made up of pressed steel members, can be considered structurally as grillages. The chassis frame consists of two side members and a number of cross members. The side and the cross-members are usually open section because of the cheap and easily to attached with rivets. The cross-members are usually attached to the side members by connection plates. The joint are riveted or bolted in trucks and are welded in trailers. Riveted joints are generally recommended for the profiles having open sections. An advantage of this connection is that increases the chassis flexibility. Therefore high stresses are prevented in critical area (Ereke,1989).

4.2 LOAD ON CHASSIS FRAME

All vehicles are subject to both static and dynamic loads which cause stresses which are limited by the design life chosen for the structure of the vehicle.

Dynamic loads result from inertia forces arising from driving on uneven surfaces. Static loads, includes maximum dynamic loads which only occur in frequently are as follows: (Beerman,1989)

*Static load of stationary vehicle.
*Braking
*Acceleration
*Cornering
*Torsion
*Maximum load on front axle which are balanced by inertia forces
*Maximum load on rear axle
*Drawbar loads from the trailer coupling system.
*Asymmetrical longitudinal loads arise from different friction forces in the off-side and near-side wheel trucks.

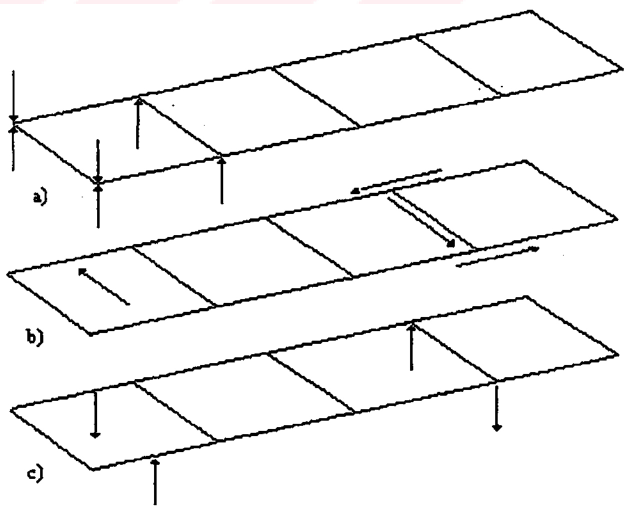

Figure 4.1 Main loads on a chassis frame.

Loads acting in the frame cause bending or torsion of the side and the cross-members. Figure 4.1 is a simplified plot of the most important kinds of load. Symmetric loads acting in the vertical direction predominantly cause bending in the side members. Vertical loads additionally arise from lateral forces acting parallel to the frame's plane, e.g. during cornering (Beerman, 1984). Loads acting in the plane of frame cause bending of the side-members and of the cross members. The most severe load of this kind arises from the cornering of trucks with tandem rear axles. Unequal tire-road adhesion in the right and left track and cornering can also cause in-plane bending. Torsion does not only occur in the simple way shown in Fig.1(c). The forces caused by wheel deflection on uneven road surface are transmitted to the side members at the bearings of the leaf springs.

4.2.1 Vertical bending

Vertical bending are due to symmetrical vertical loads, static loads of a stationary vehicle, braking and acceleration loads, inertial loads causing by bumps.

The chassis frame of two axle vehicles and vehicles with balance-beam twin rear axles are treated as simply supported beams. The support loads from the axes are distributed through the spring hangers, as shown in Figure.4.2 (Beerman, 1989)

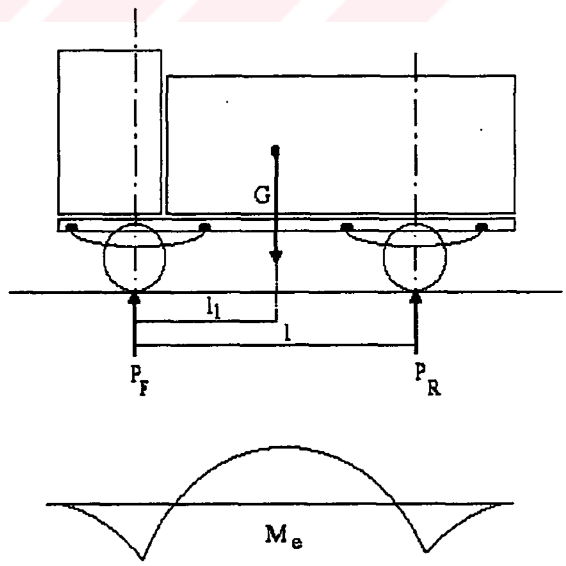

Figure 4.2. Axle Load and Bending moment diagram

Figure 4.3 shows the loads act on a vehicle under a braking deceleration (Ereke,1989) . Bending moments can be written as

$$M_1 = -q\frac{x^2}{2} + aqxh$$
$$M_2 = -q\frac{x^2}{2} + P_A(x - l_1) + aqxh \qquad (4.1)$$

Braking and acceleration moments cause pitching moments which have to be transferred to the frame as vertical loads through the spring hangers, the resulting bending moments act at the neutral axes of the frame side members. These bending moments are shown in Figure 4.4.

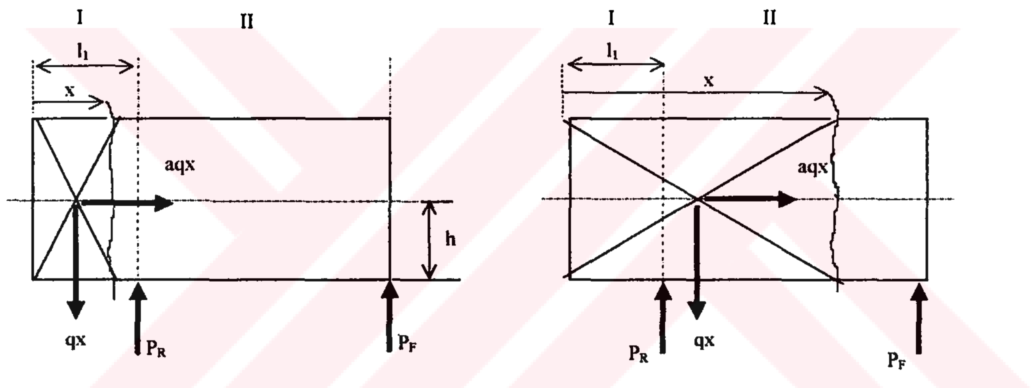

Figure 4.3. Trucks under a braking deceleration

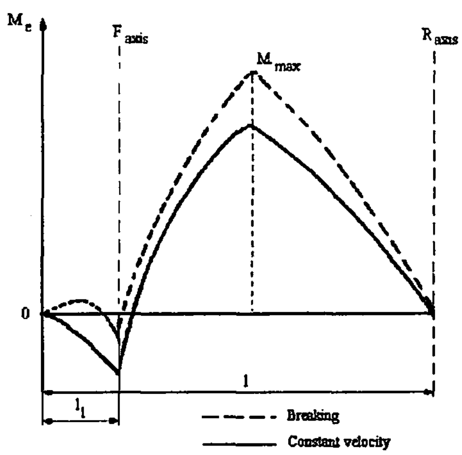

Figure 4.4. Bending moment diagrams under a braking deceleration

The extreme loads caused by bumps are subjected to the frame in vertical direction also (Ereke 1989). As shown in Figure 4.5 the force A_{Hst} at the rear axle causes a vertical acceleration of the center of gravity of the sprung mass m_2 which is given by

$$z_2 = A_{Hst} / m_2 \tag{4.2}$$

and the pitching acceleration about the lateral axis through the center of gravity is

$$\varepsilon_2 = l_{H2} A_{Hst} / \theta_{2y} \tag{4.3}$$

where θ_{2y} is the pitching moment of inertia of the sprung mass and the forces and dimensions are shown in Figure 4.5

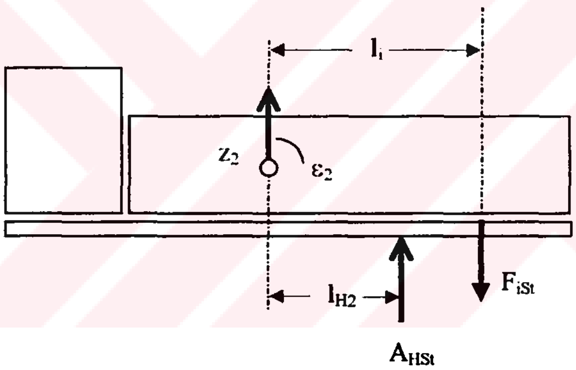

Figure 4.5. The effect on the load at load point i of the rear axle hitting a bump.

This approximation is sufficiently accurate because the change in the front spring force during the impact of the rear wheel with the bump is negligible.

The increment of the force at load point i can be written as

$$F_{ist} = m_i(z_2 + l_i\varepsilon_2) \text{ or } F_{ist} = m_i(1/m_2 + l_{H2}l_i / \theta_{2y})A_{Hst} \tag{4.4}$$

Thus, static bending moment over the rear axle increases.

4.2.2 Horizontal Bending

Horizontal bending arise from cornering forces or asymmetrical longitudinal forces, scrubbing of non-steerable double axles.

Because of the center of gravity of the load is above the chassis frame the lateral acceleration due to cornering increases the load on the side member on the outside of the curve. This effect is illustrated in Figure 4.6 where the lateral acceleration is taken as a times gravity, and the increment in the force becomes $aF_ih_is_i/b$. It is sufficient to increase all the static loads on this side of the vehicle by same factor, unequal loads along the length of the vehicle will result in some torsion being applied to the frame but, on the whole, this torque can be neglected.

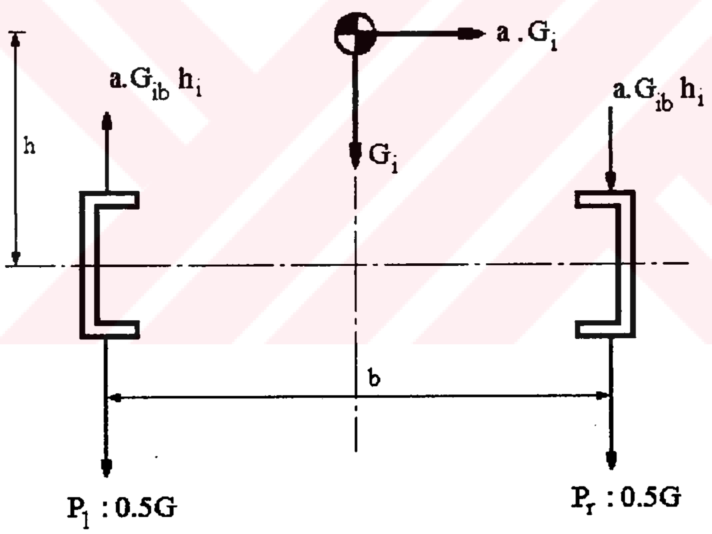

Figure 4.6. Vertical loads at load point i during cornering with lateral acceleration of aG_i

4.2.3 Torsion

Maximum torsion case is found when one wheel of the most lightly loaded axle is hanging free while the other is on a bump and both wheels of the other axle are on a flat surface.

The difference between the right and left wheel axle load forced the chassis by torsion along the longitudinal axes. The difference of the axles load according to each other the amount of the torsional moment are dependent the following reasons (Beerman 1989).

*Height of a bump

Torsion moment increases depending on the height of a bump. This height of bump is limited ±30cm for trucks.

*Wheel Trace Length

The more wheel trace length is, the less the torsion moment for a given height of a bump will be.

*Stiffness of the springs and wheels

If springs and wheels are flexible, the torsion will be less.

*Stiffness of the frame

The moment decreases with the increasing flexibility of the body.

CHAPTER FIVE

DEFINITION OF THE PROBLEM

5.1 INTRODUCTION

In this study stress analysis of riveted joints of truck chassis frames was conducted under different road conditions .

Two types of chassis frame was considered. The difference between them is the spring hangers of the rear axles. While the chassis model (1) has a fixed spring hanger, the chassis model (2) has movable spring hanger.

First , stress analysis of two types of chassis frame was conducted three different road condition.

Road case (1); all the wheel are on a flat surface.

Road case (2);one wheel of the rear axle is free while the other axles are on a flat surface.

Road case(3); one wheel of the front axle is free while the other axles are on a flat surface.

Then using submodeling technique(Appendix B) the riveted joints between a cross member and a side member has been analyzed.

Finally, most stressed joints were compared for two types of chassis frame. The effect of the connection plate thickness, length and shape was investigated.

5.2 CONSTRUCTION OF THE THEORETICAL MODEL

The general arrangement of the chassis frames model (1) which has a fixed spring hanger, and model(2) which has movable spring hanger. investigated are shown in Figure 5.1. The overall of the frame does not include local details such as fillet radii.

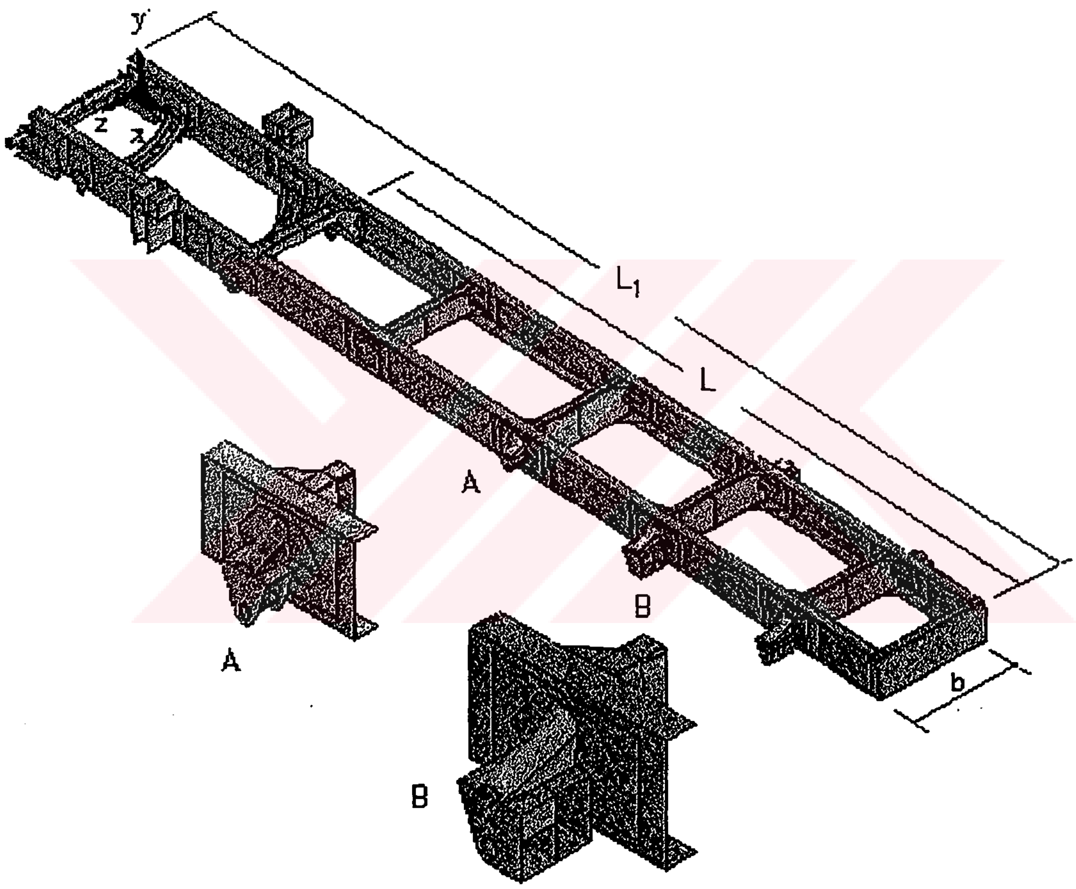

Figure 5.1.a.- Chassis frame model(1) which has a fixed spring hanger.

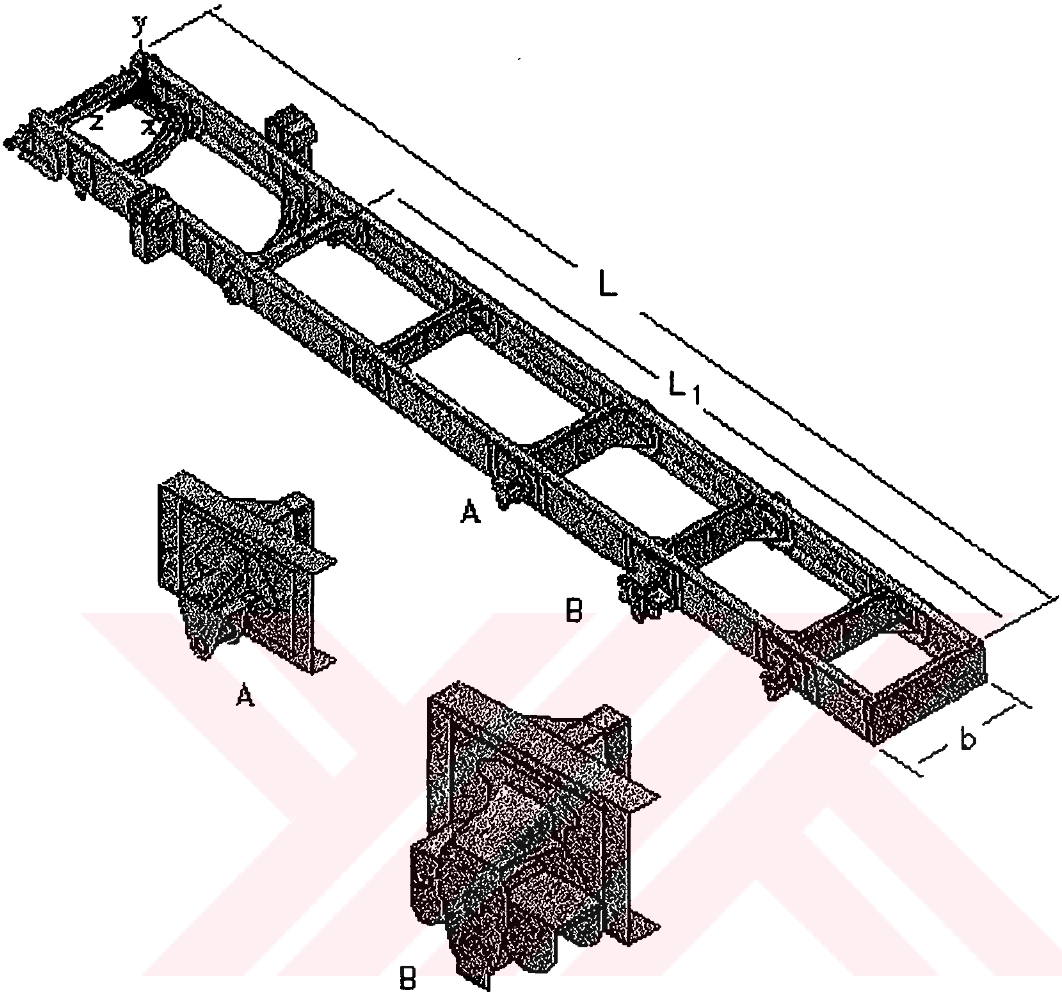

Figure 5.1.b. Chassis frame model(2) which has a movable spring hanger.

Where

L= Length of the chassis

L_1=Active load length

B= Width of the chassis

5. 3 FINITE ELEMENTS MODEL AND BOUNDARY CONDITIONS

In the solution two dimensional isoparametric elements are used. Finite element models of the riveted joint consist of 8000 nodes. Upper and lower plates by a rivet in Figure 5.4. are modeled with plate/shell elements. Plates are overlapped by the boundary of the rivet surroundings to ensure equal displacements. Riveted joint on frame model 2 are shown detailed in Figure 5.2 .

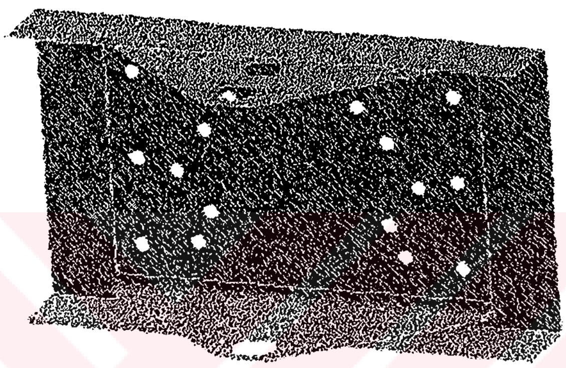

Figure 5.2. Upper and Lower Plates

Boundary conditions in load case(1) are shown in Figure 5.3. Loads on frame are given in Table5.1

Table 5.1 Loads on a chassis frame

Cab Weight	Engine Weight	Chassis Weight	Load
7000N	4800N	46200N	213800N

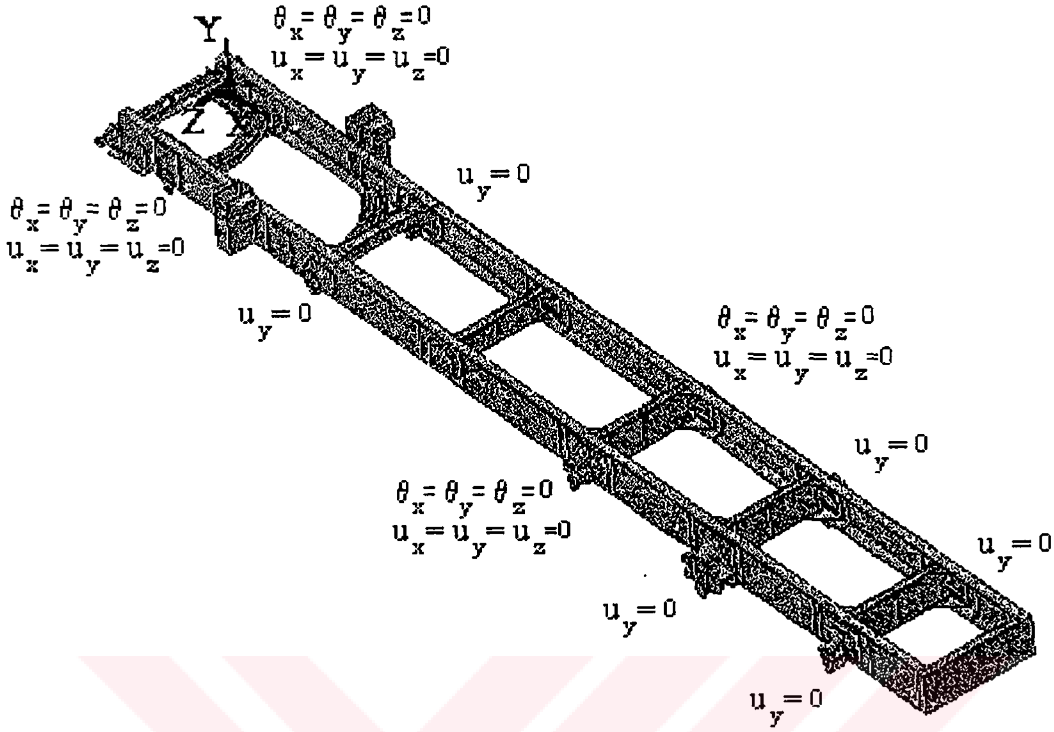

Figure.5.3 Boundary conditions on a chassis model 2, for road case(1).

5.4 MATERIAL PROPERTIES OF THE TRUCK CHASSIS

The material properties of a chassis are given in Table 5.2.

Table 5.2. Material Properties.

Material	Elasticity Modulus	Poisson's Ratio	Yield Point
St52	210000 Mpa	0.3	350MPa

CHAPTER SIX
RESULTS AND DISCUSSION

The riveted joints between a cross member and a side member has been analyzed using a finite elements method . The maximum principal stresses where found for different road conditions.

The finite element results for the maximum principal stress distribution were given in the section across (*) the flanges of the beams shown in Figure 6.1.

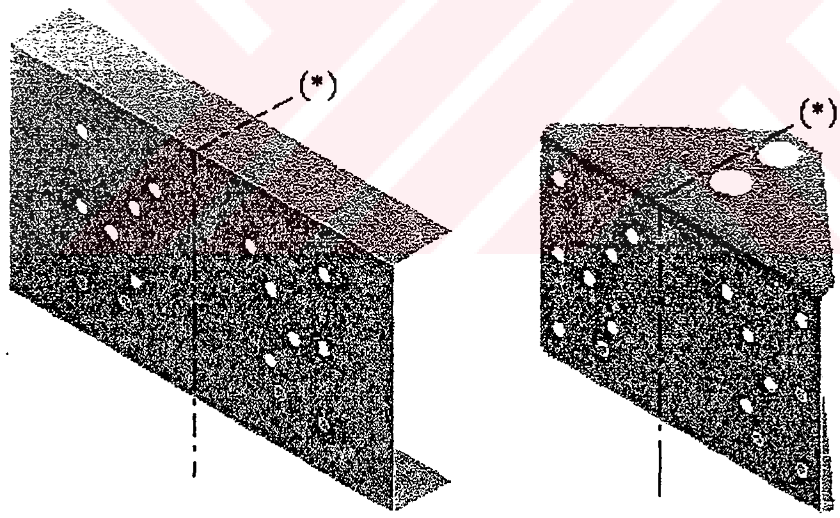

Figure 6.1 Section across the flanges of beams denoted by(*). a). Cross section across the side member is denoted by(*). b). Cross section across the connection plate is denoted by(*)

Results obtained this study are as follows:

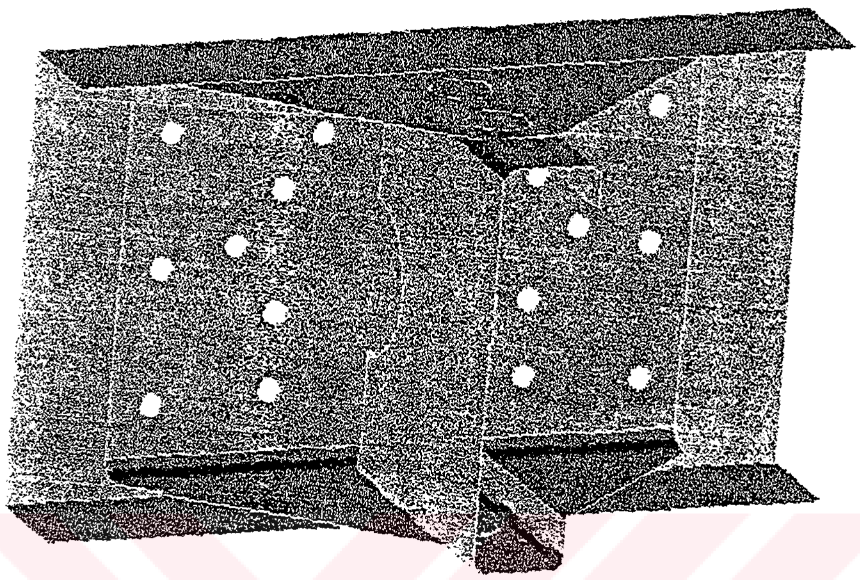

A

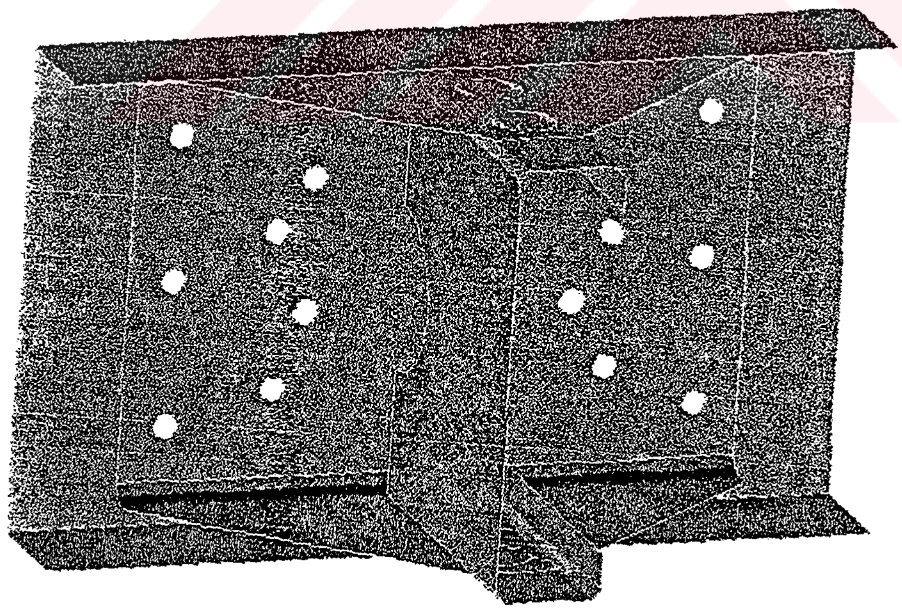

B

Figure 6.2. Joint A and B for the chassis model (1) which has a fixed spring hanger.

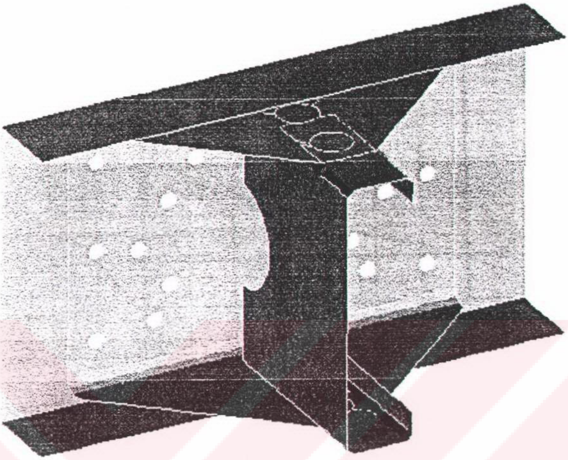

A

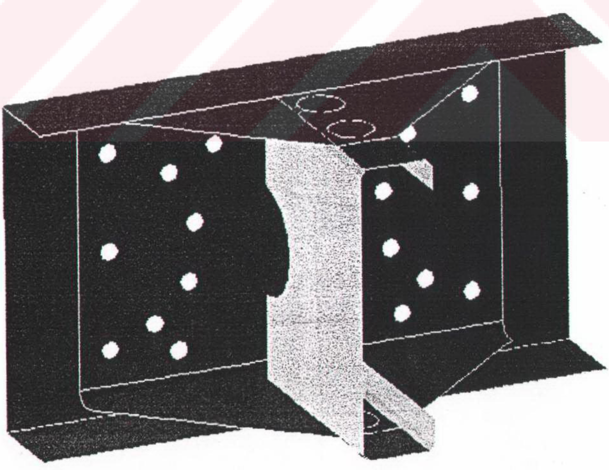

B

Figure 6.3. Joint A and B for the chassis model (2) which has a movable spring hanger

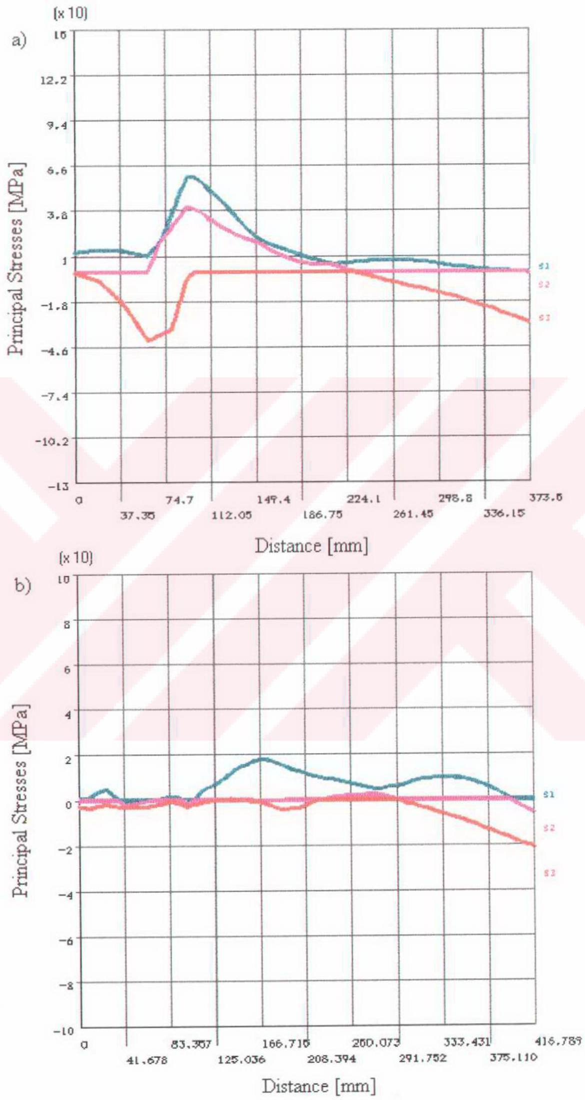

Figure 6.4. Stress distribution of a joint A for the chassis model 1, at the sections shown in Figure 6.1, in road case1.

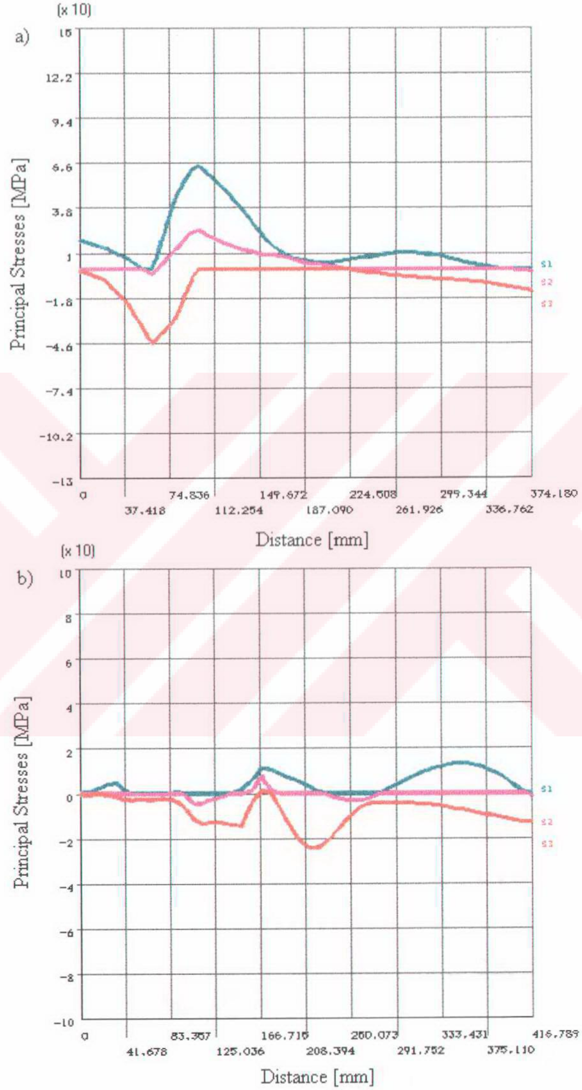

Figure 6.5. Stress distribution of a joint B for the chassis model 1, at the sections shown in Figure 6.1, in road case 1.

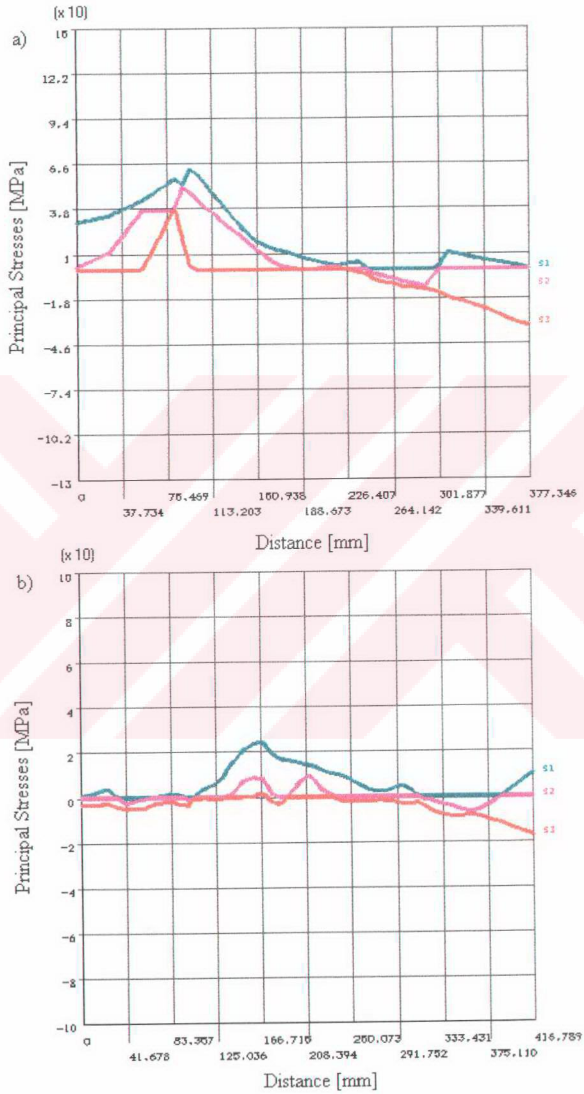

Figure 6.6. Stress distribution of a joint A for the chassis model 2, at the sections shown in Figure 6.1, in road case 1.

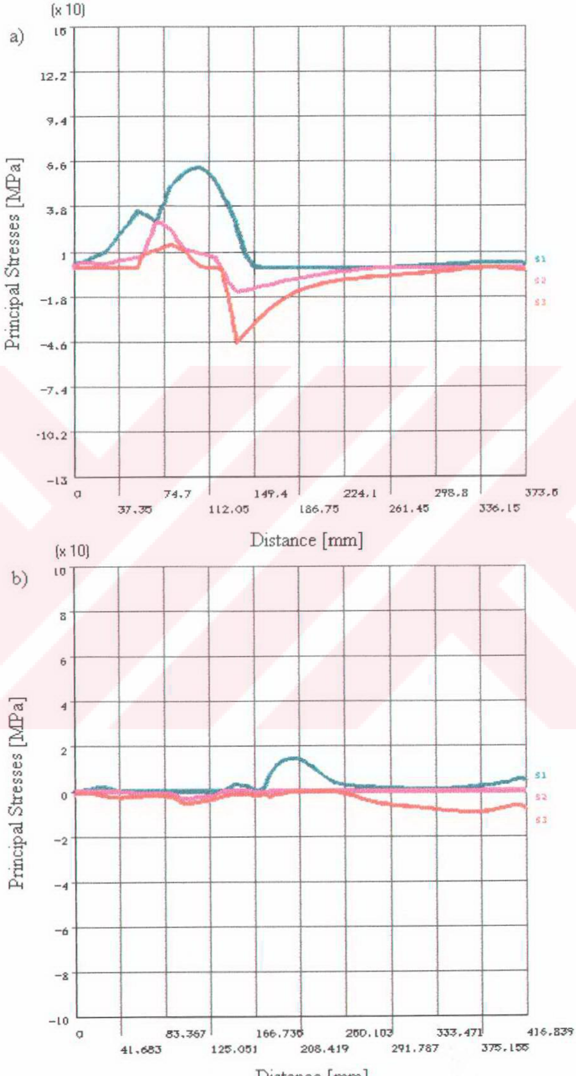

Figure 6.7. Stress distribution of a joint B for the chassis model 2, at the sections shown in Figure 6.1, in road case 1.

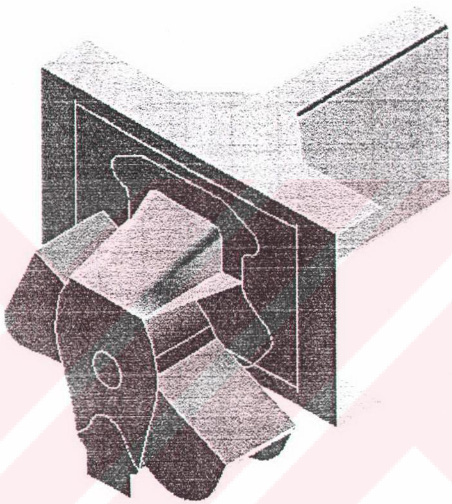

Figure 6.8. Joint B on a chassis model 2, in road case 2.

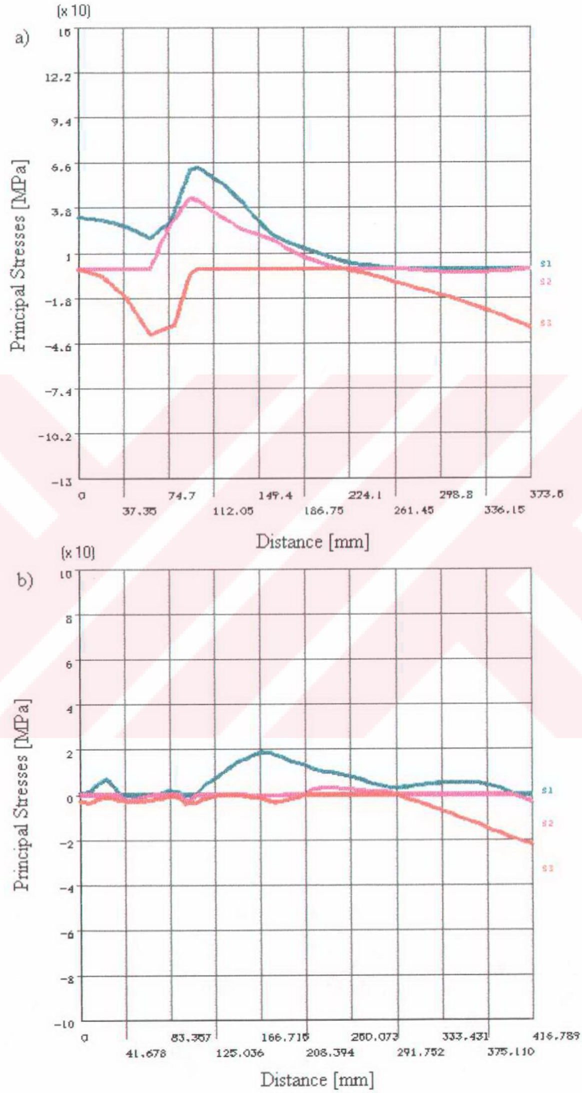

Figure 6.9. Stress distribution of a joint A for the chassis model 1, at the sections shown in Figure 6.1, in road case 2.

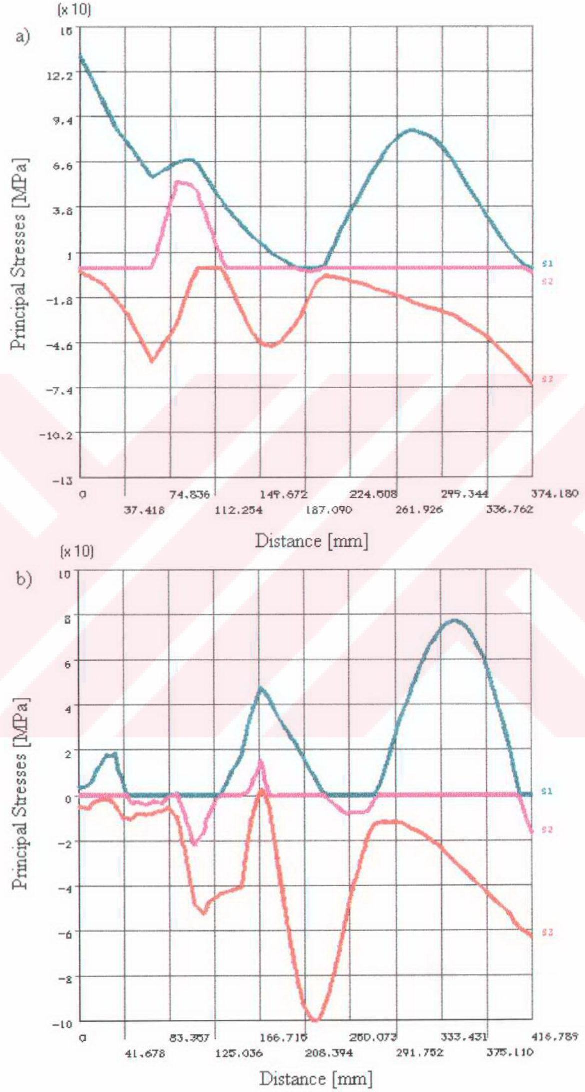

Figure 6.10. Stress distribution of a joint B for the chassis model 1, at the sections shown in Figure 6.1, in road case 2.

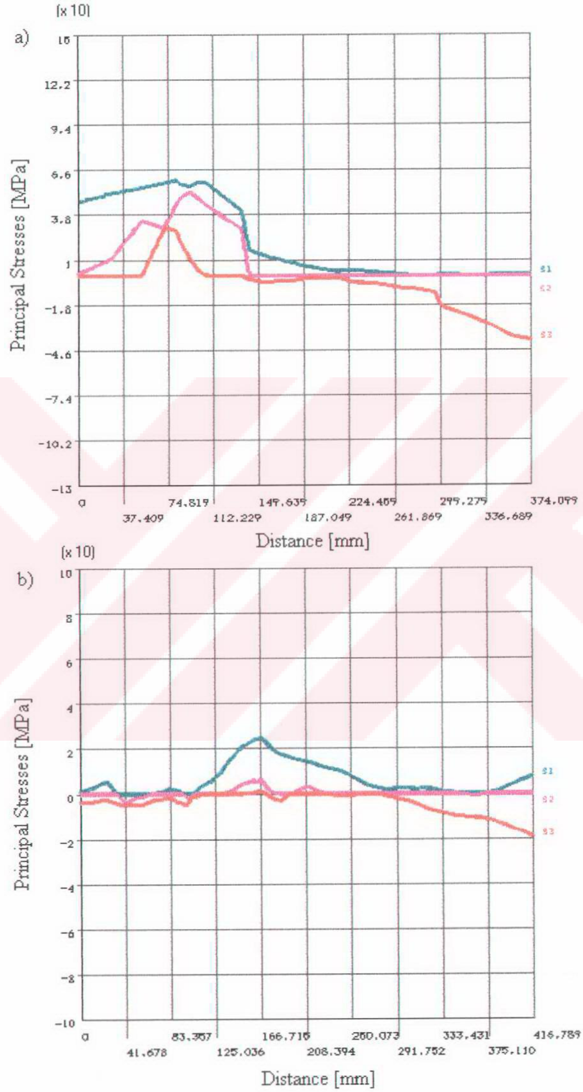

Figure 6.11. Stress distribution of a joint A for the chassis model 2, at the sections shown in Figure 6.1, in road case 2.

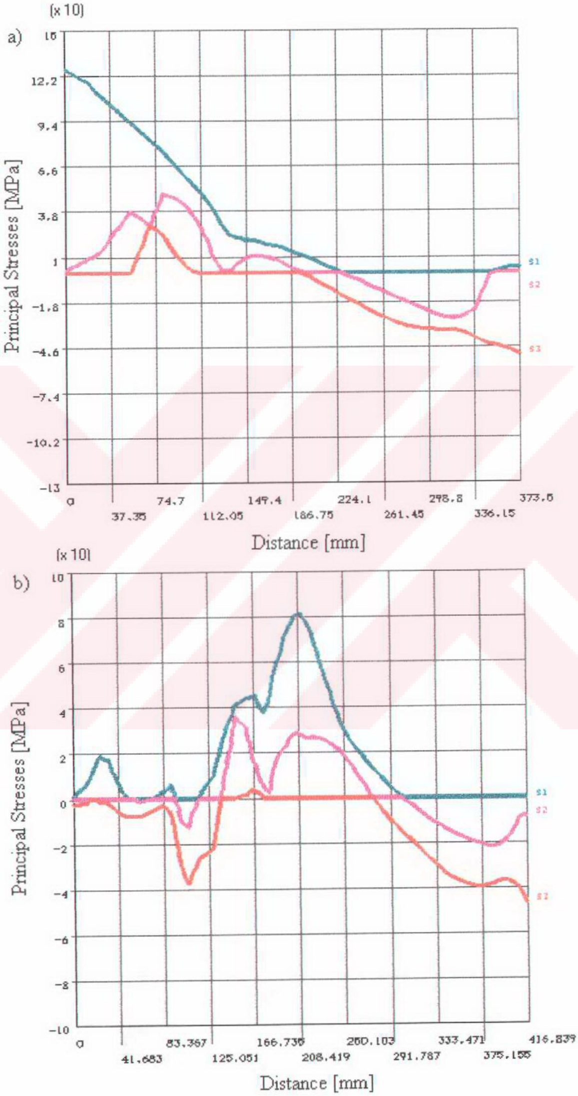

Figure 6.12. Stress distribution of a joint B for the chassis model 2, at the sections shown in Figure 6.1, in road case 2.

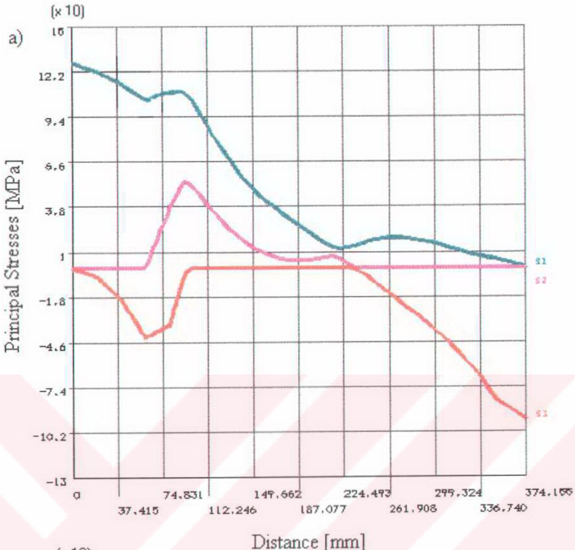

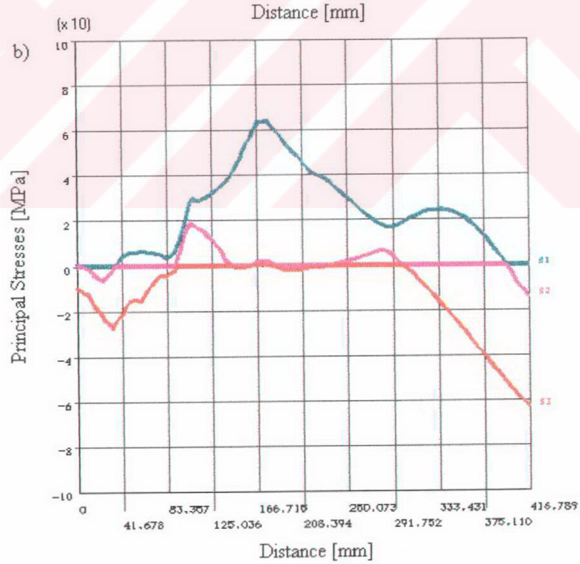

Figure 6.13. Stress distribution of a joint A for the chassis model 1, at the sections shown in Figure 6.1, in road case 3.

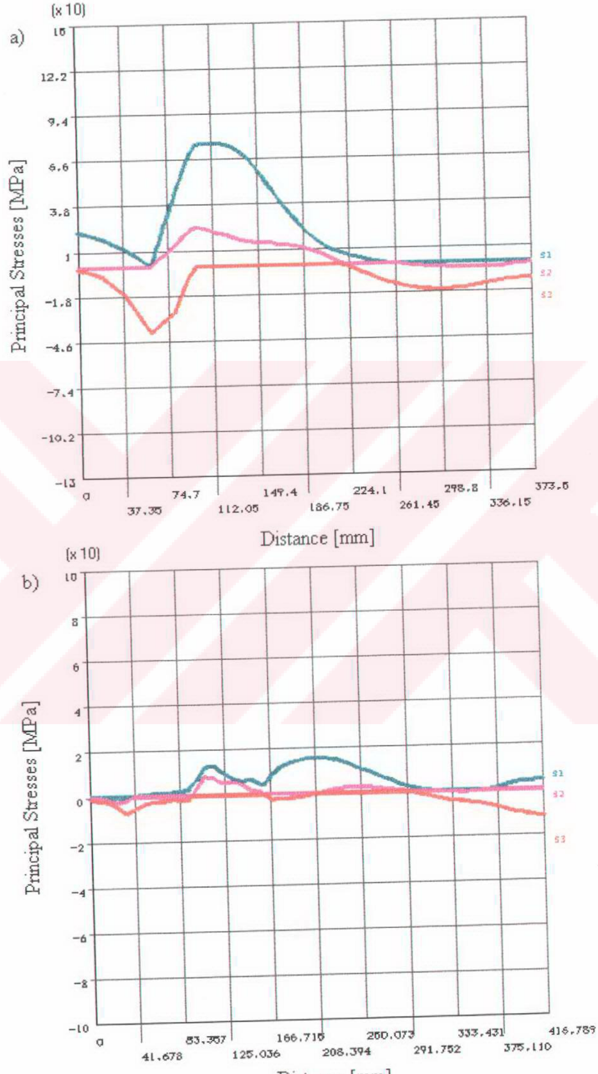

Figure 6.14. Stress distribution of a joint B for the chassis model 1, at the sections shown in Figure 6.1, in road case 3.

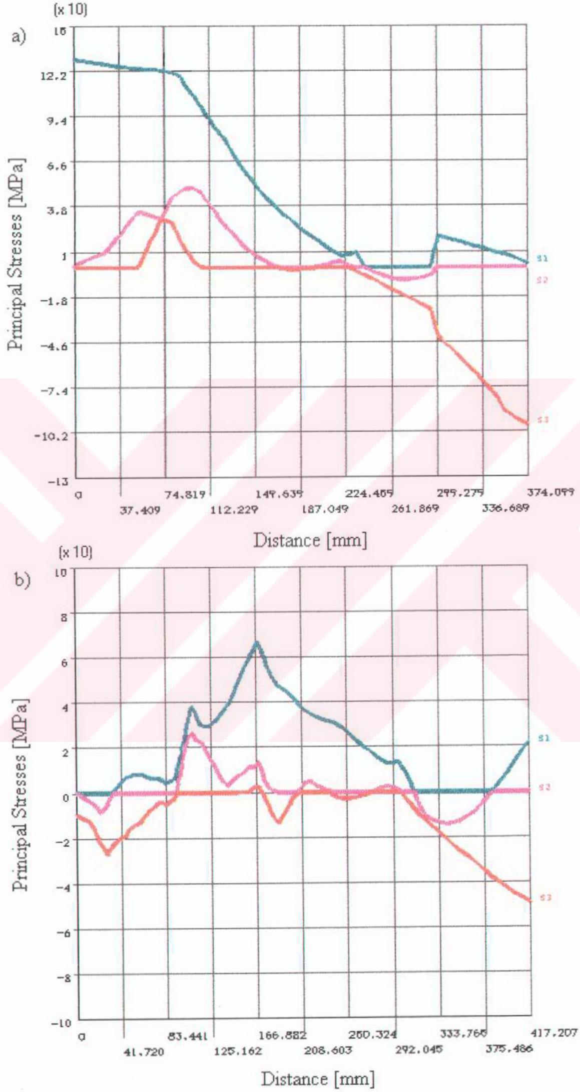

Figure 6.15. Stress distribution of a joint A for the chassis model 2, at the sections shown in Figure 6.1, in road case 3.

a)

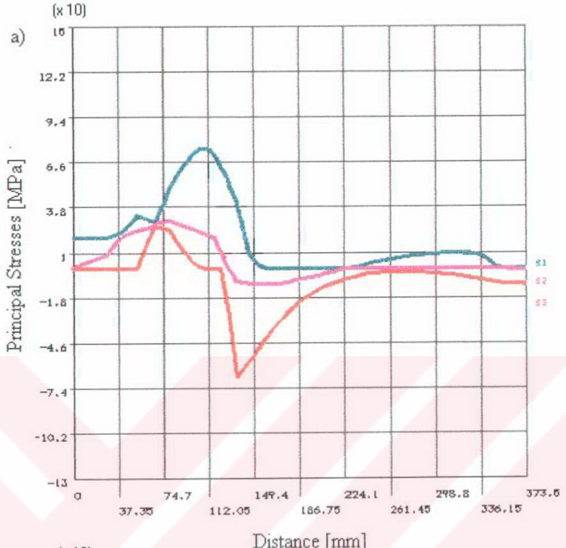

b)

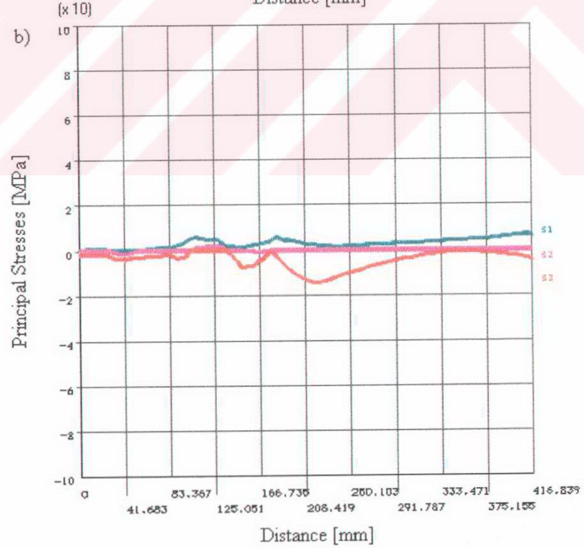

Figure 6.16. Stress distribution of a joint B for the chassis model 2, at the sections shown in Figure 6.1, in road case 3.

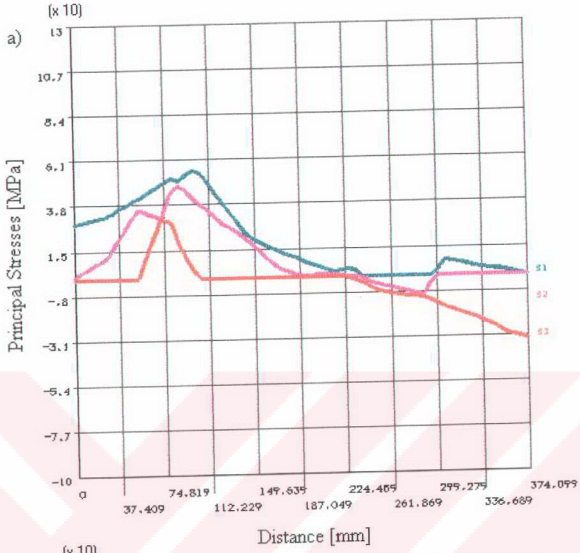

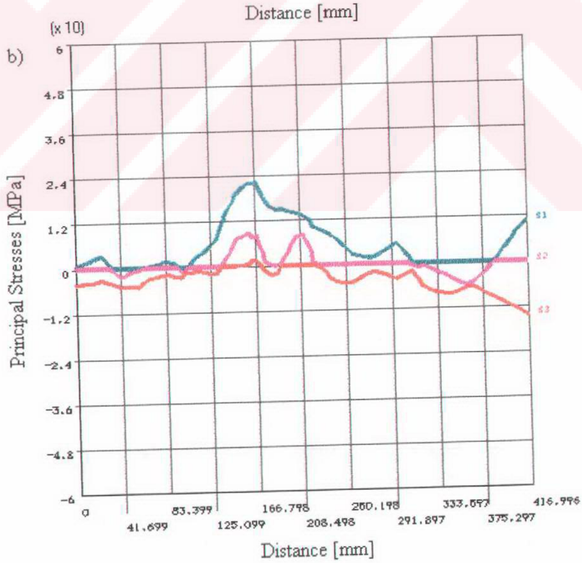

Figure 6.17. Stress distribution of a joint at the sections shown in Fig.6.1, for connection plate thickness t=8mm, in road case1.

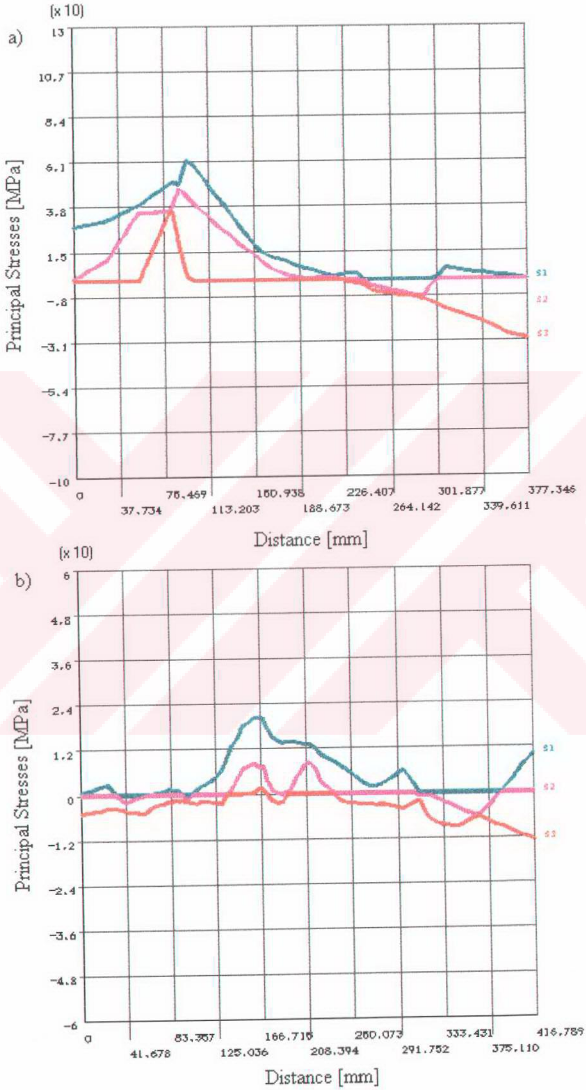

Figure 6.18. Stress distribution of a joint at the sections shown in Fig.6.1, for connection plate thickness t=10 mm, in road case 1.

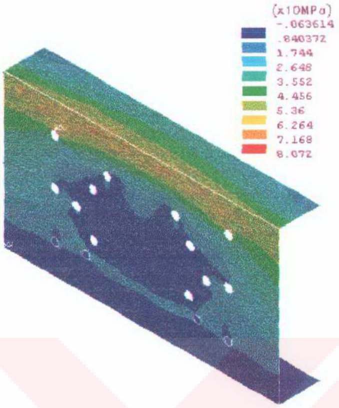

Side member thickness=8 mm

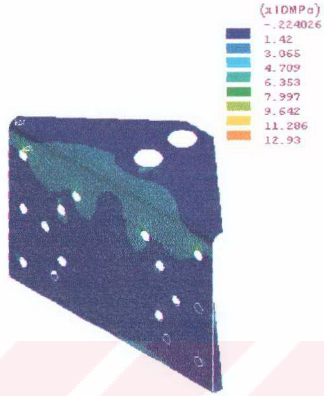

Connection plate thickness t=6 mm

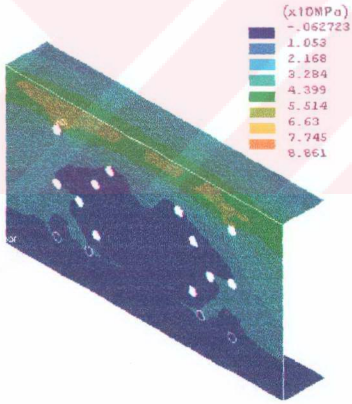

Side member thickness=8 mm

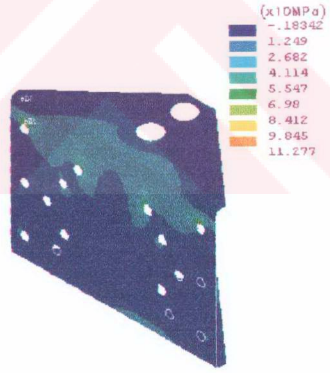

Connection plate thickness t=8 mm

Figure 6.19. Maximum principal stress contour on a side member and the connection plate, for road case1.

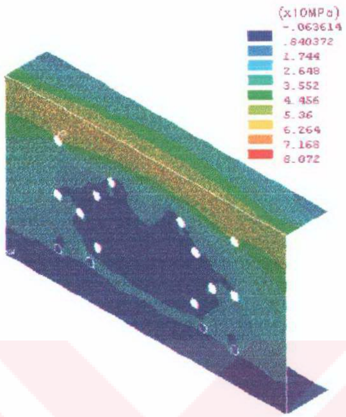

Side member thickness=8 mm

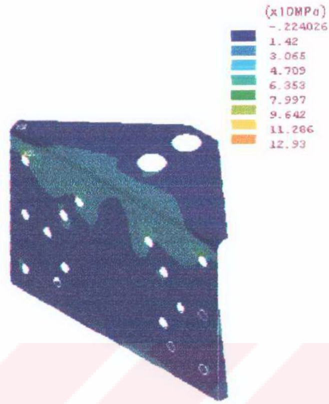

Connection plate thickness t=6mm

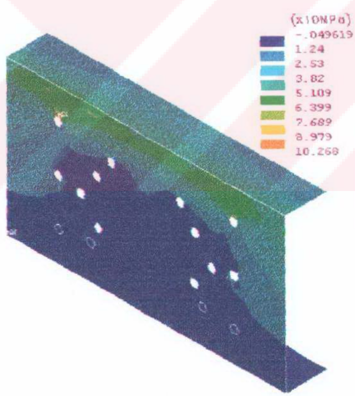

Side member thickness=8 mm

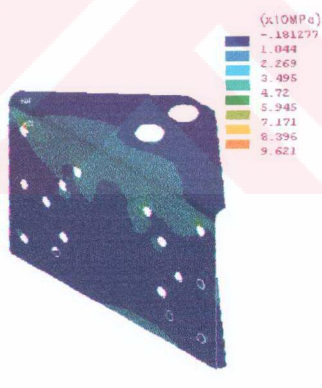

Connection plate thickness t=10mm

Figure 6.20. Maximum principal stress contour on a side member and a connection plate, for road case1.

a)

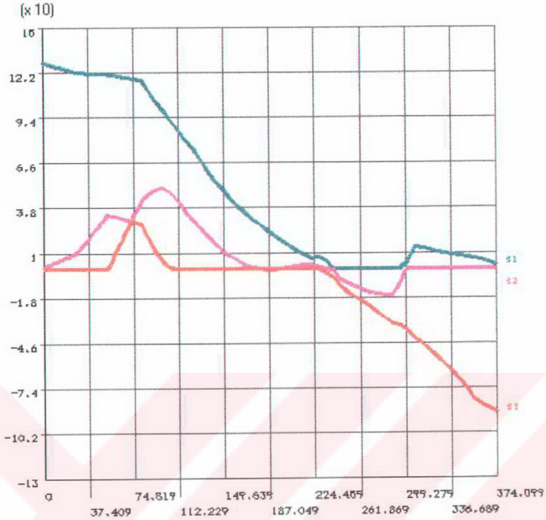

b)

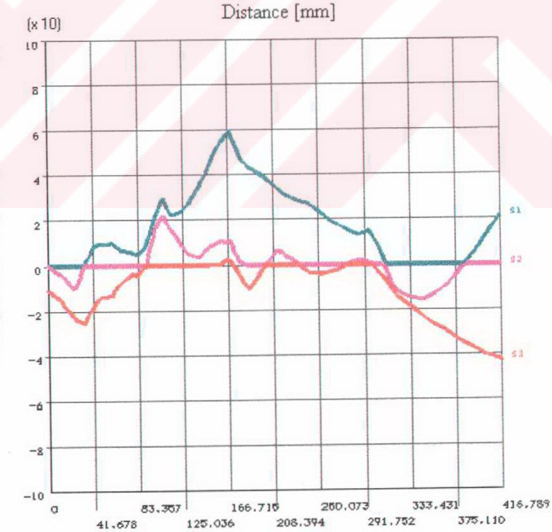

Figure 6.21. Stress distribution of a joint at the sections shown in Fig.6.1, for connection plate thickness t=8 mm, in road case 3.

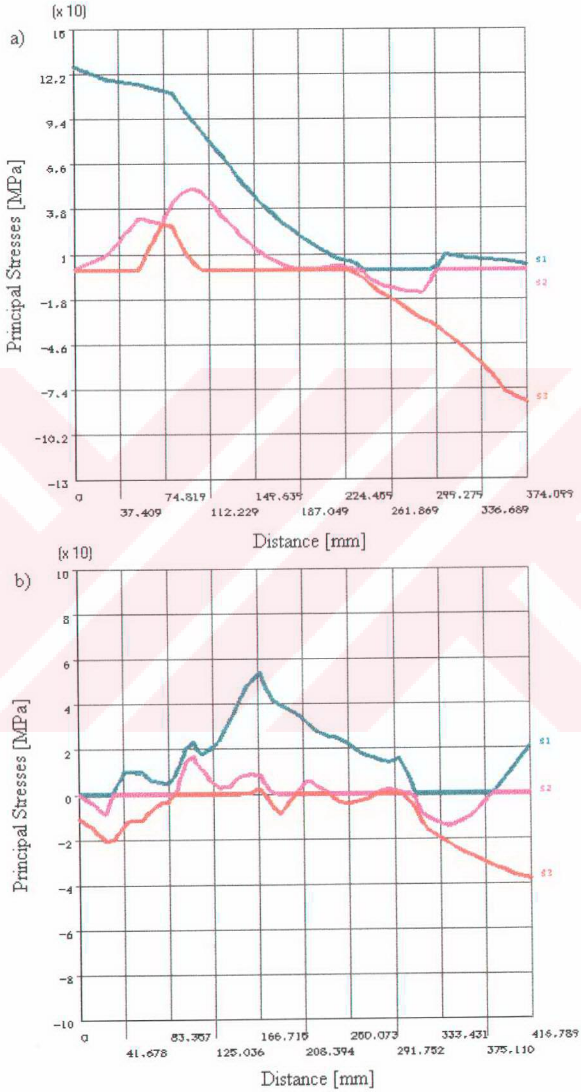

Figure 6.22. Stress distribution of a joint at the sections shown in Fig.6.1, for connection plate thickness t=10 mm, in road case 3.

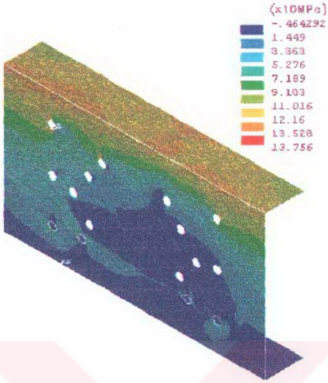

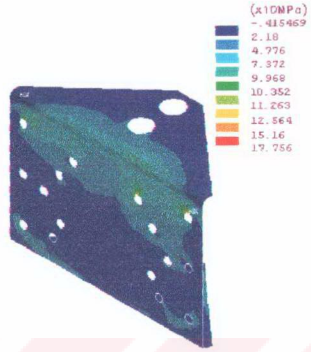

Side member thickness=8 mm

Connection plate thickness t=6mm

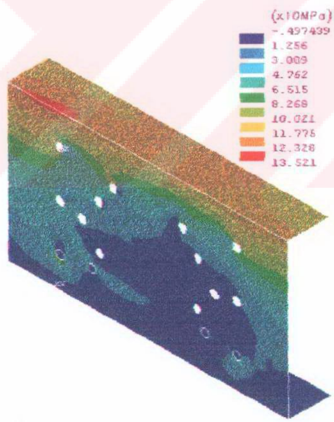

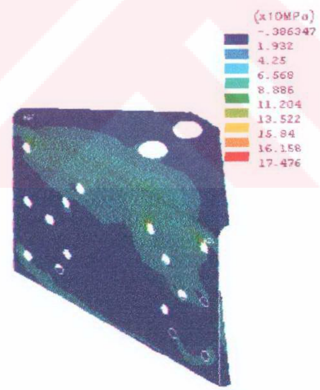

Side member thickness=8 mm

Connection plate thickness t=8mm

Figure 6.23. Maximum principal stress contour on a side member and a connection plate, for road case 3.

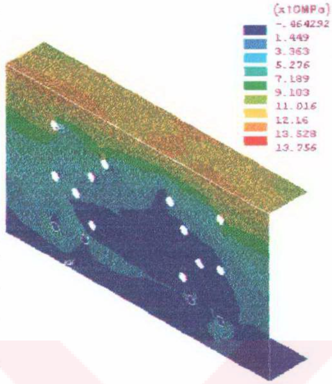

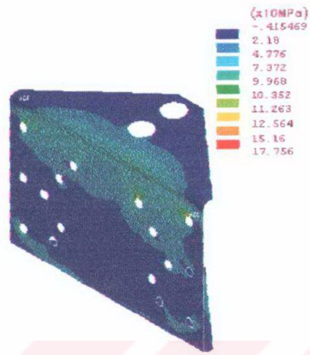

Side member thickness=8 mm

Connection plate thickness t=6mm

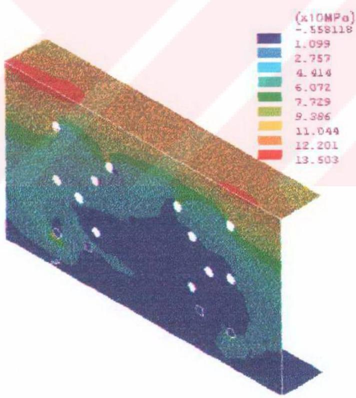

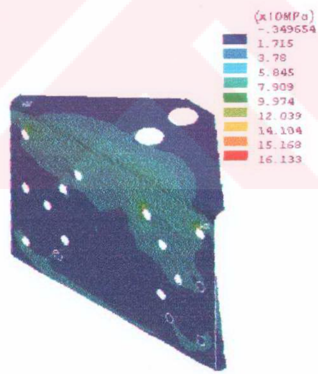

Side member thickness=8 mm

Connection plate thickness t=10mm

Figure 6.24. Maximum principal stress contour on a side member and a connection plate, for road case3.

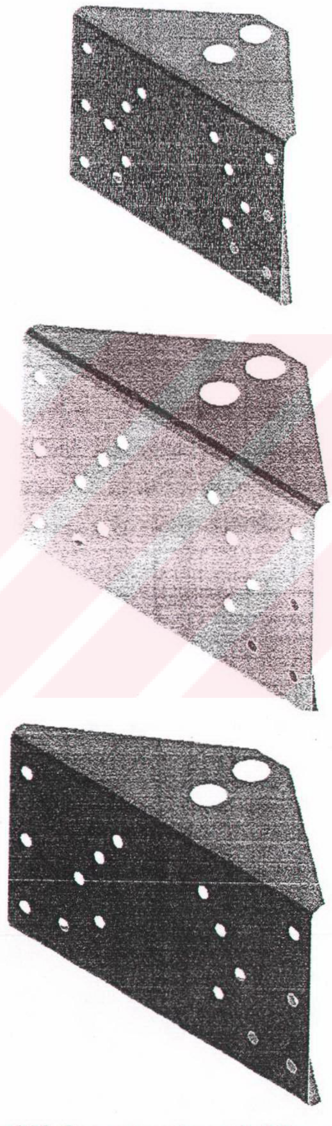

Figure 6.25 Connection plate with different length

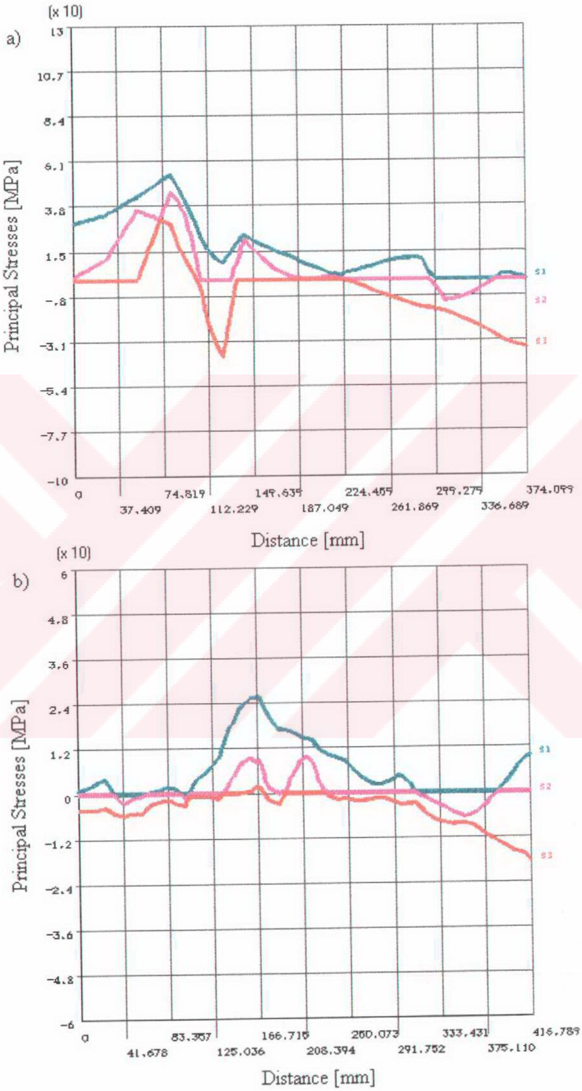

Figure 6.26. Stress distribution of a joint at the sections shown in Fig.6.1, for the connection plate length l=430mm, in road case1.

a)

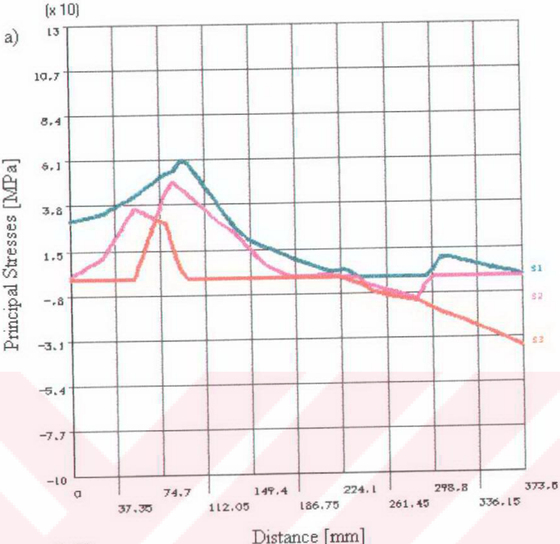

b)

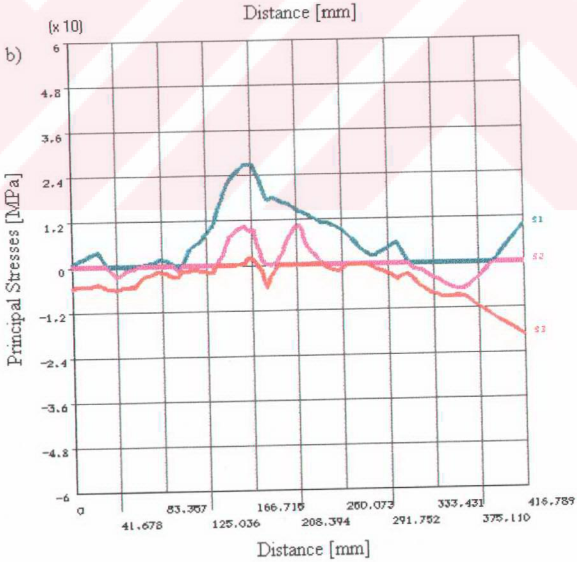

Figure 6.27. Stress distribution of a joint at the sections shown in Fig.6.1, for the connection plate length l=470mm, in road case 1.

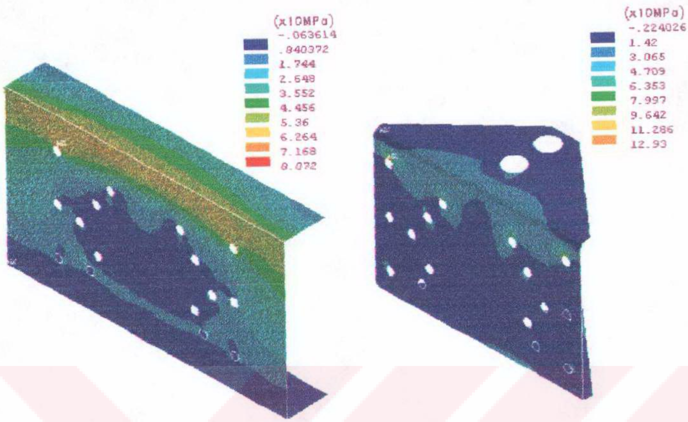

Connection plate length l=390mm

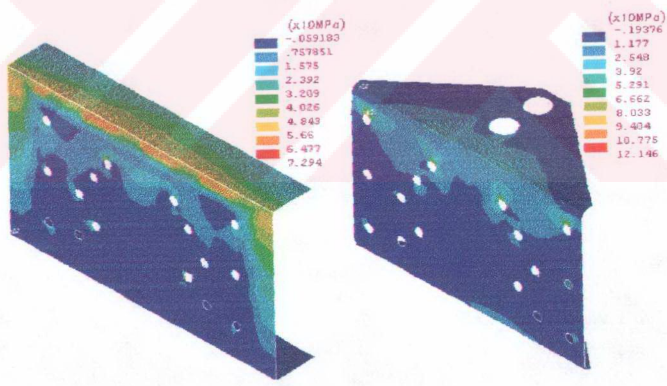

Connection plate length l=430 mm

Figure 6.28. Maximum principal stress contour on a side member and a connection plate, for road case 1.

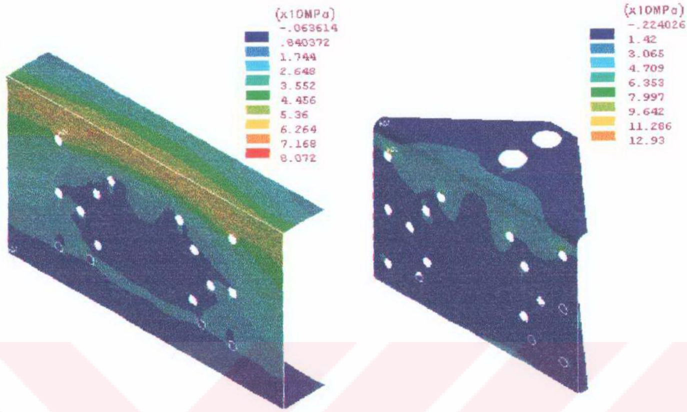

Connection plate length l=390mm

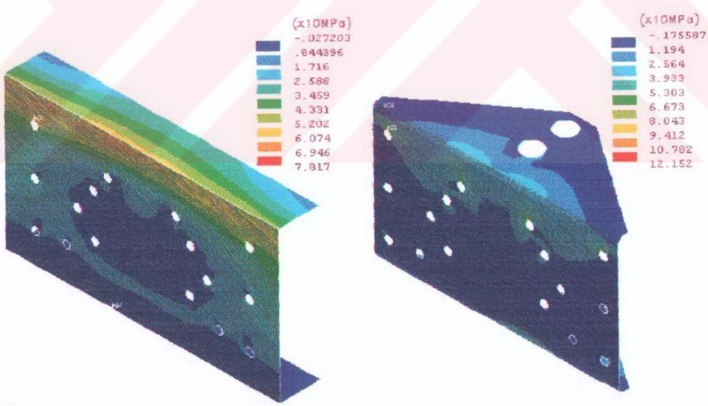

Connection plate length l=470mm

Figure 6.29. Maximum principal stress contour on a side member and a connection plate, for road case1.

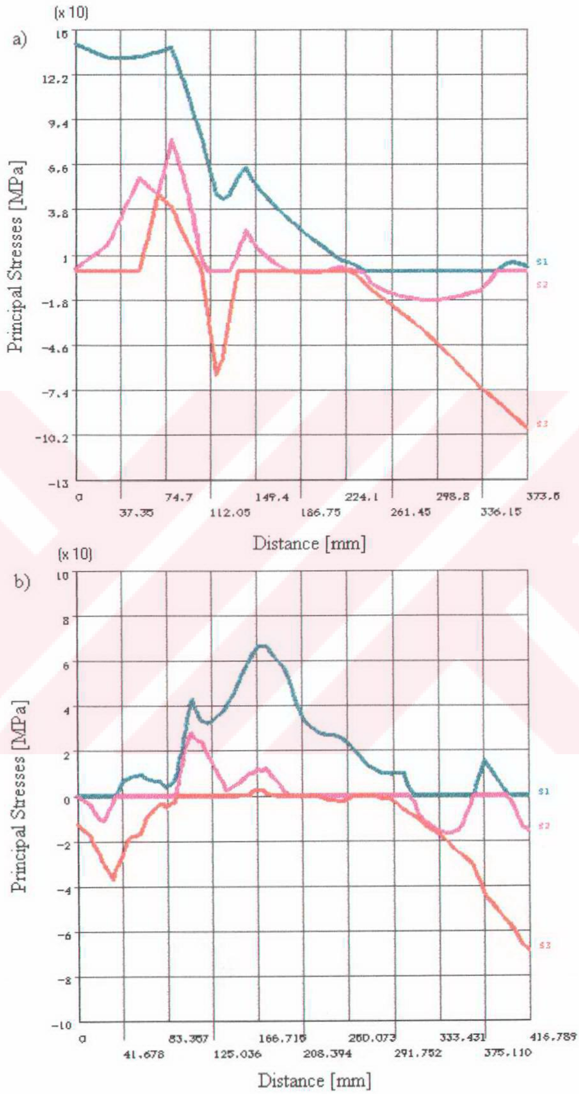

Figure 6.30. Stress distribution of a joint at the sections shown in Fig.6.1, for the connection plate length l=430mm, in road case 3.

a)

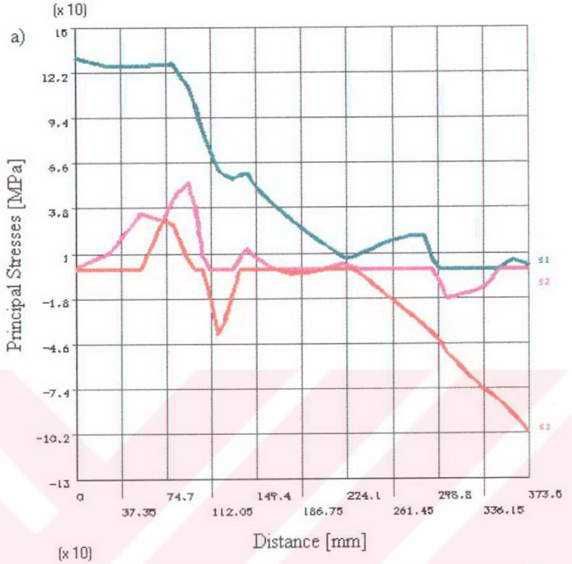

b)

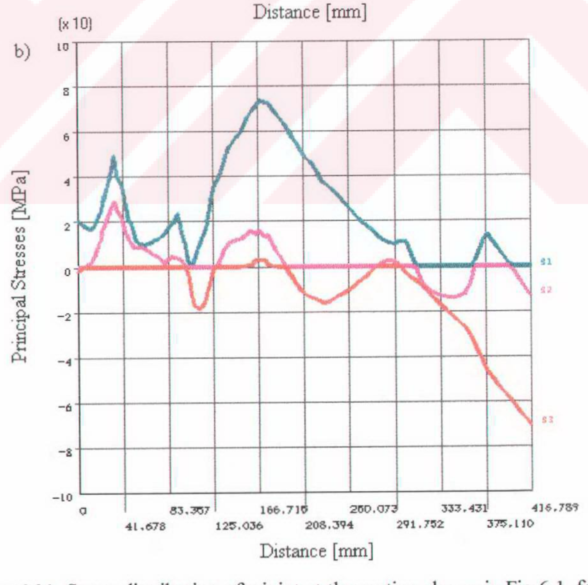

Figure 6.31. Stress distribution of a joint at the section shown in Fig.6.1, for the connection plate length l=470mm, in road case 3.

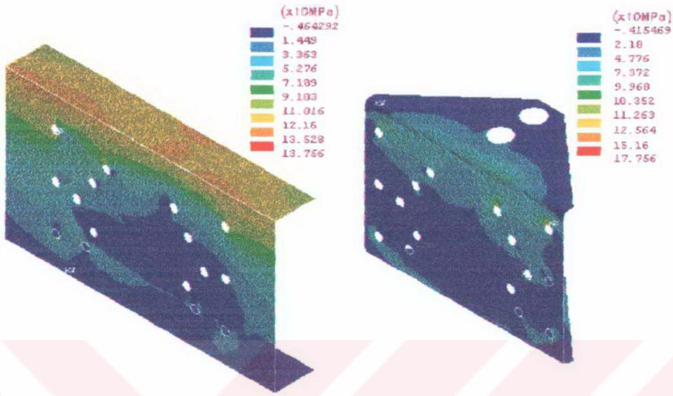

Connection plate length 390 mm

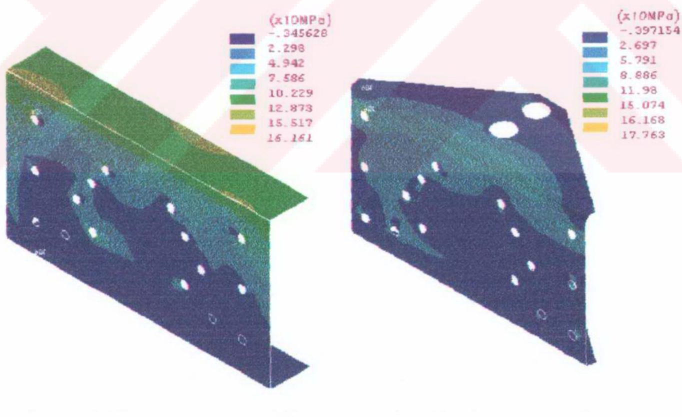

Connection plate length l=470 mm

Figure 6.32. Maximum principal stress contour on a side member and a connection plate, for road case 3.

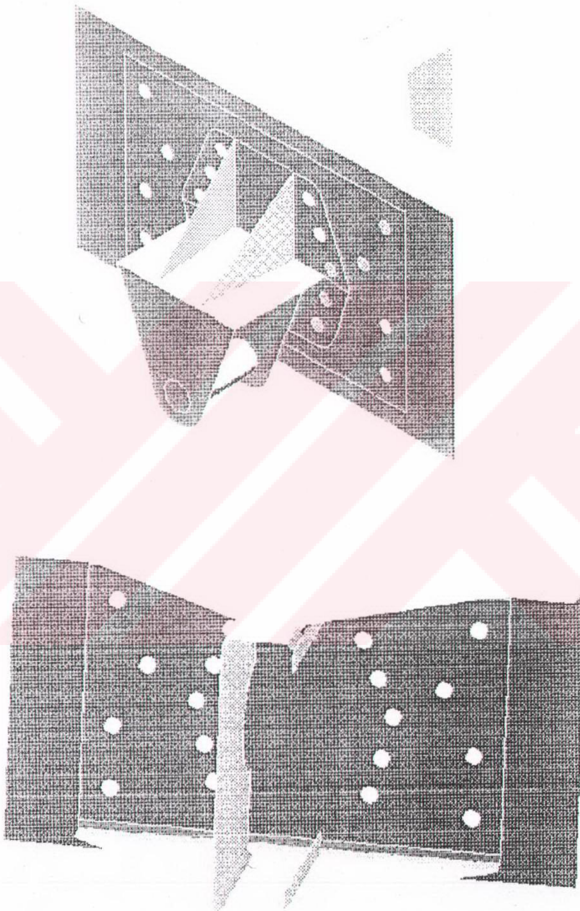

Figure 6.33 Joint model A1. The spring hanger shape and the rivet locations are changed.

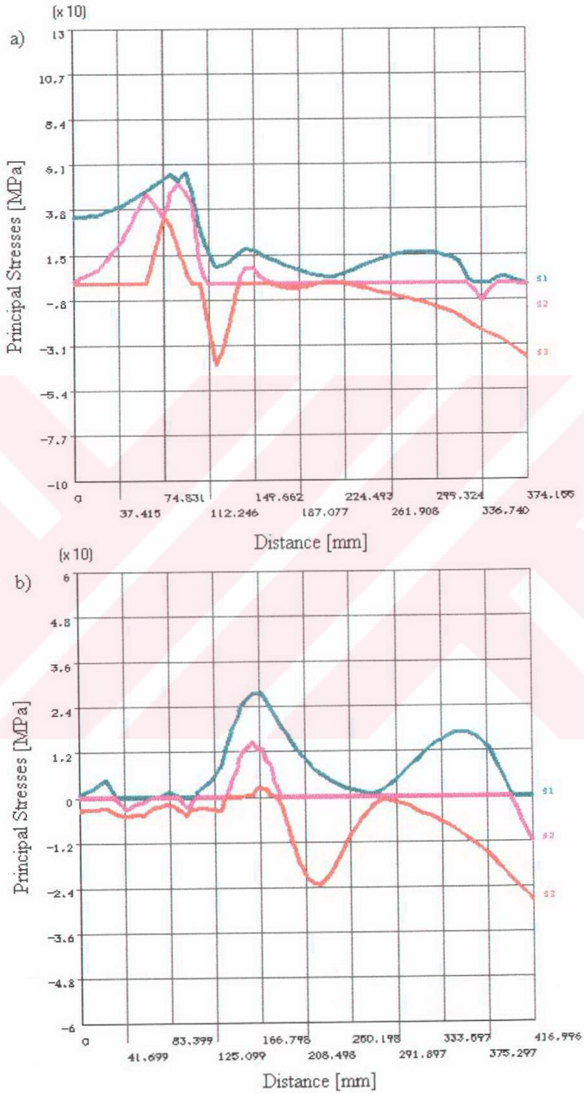

Figure 6.34. Stress distribution of a joint A1, at the sections shown in Fig.6.1, in road case 1.

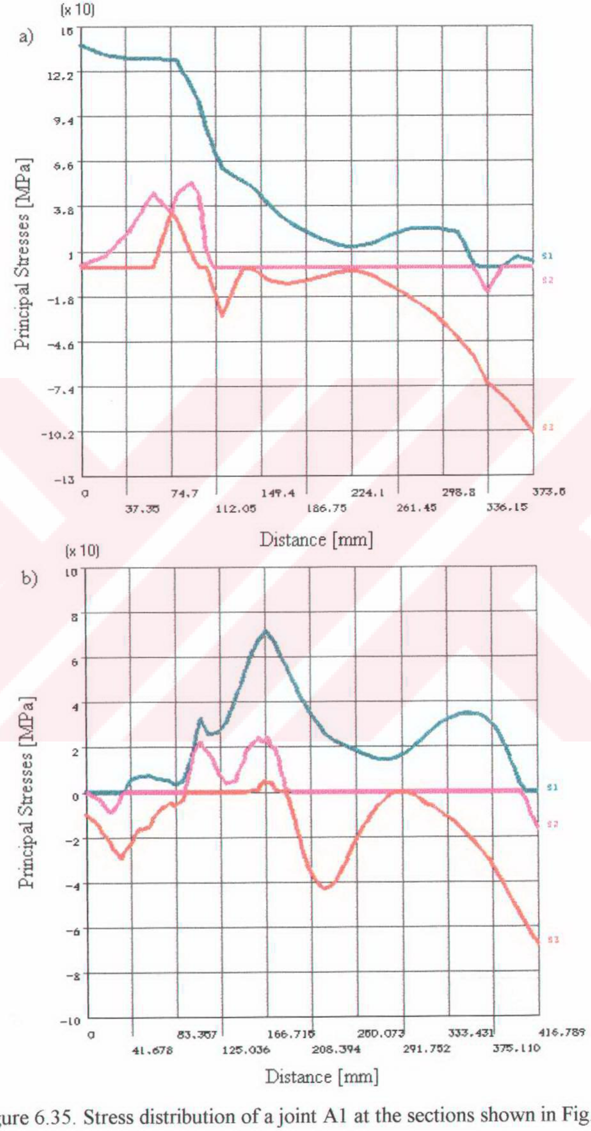

Figure 6.35. Stress distribution of a joint A1 at the sections shown in Fig.6.1, in road case 3.

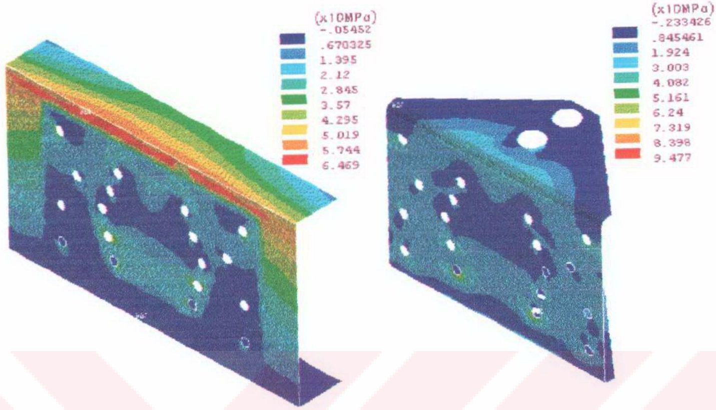

road case 1

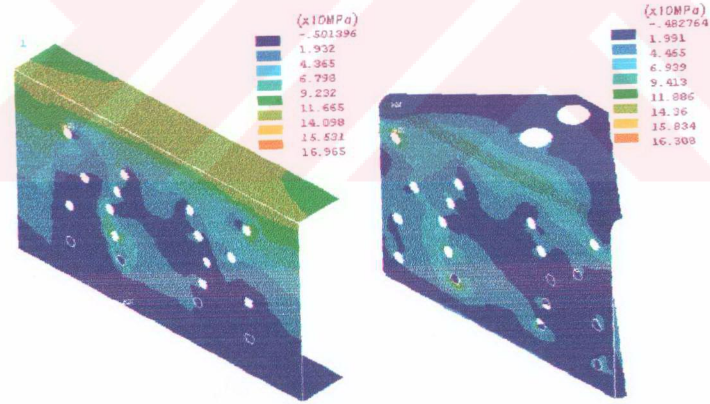

road case 3

Figure 6.36. Maximum principal stress contour on a side member and a connection plate for joint A1

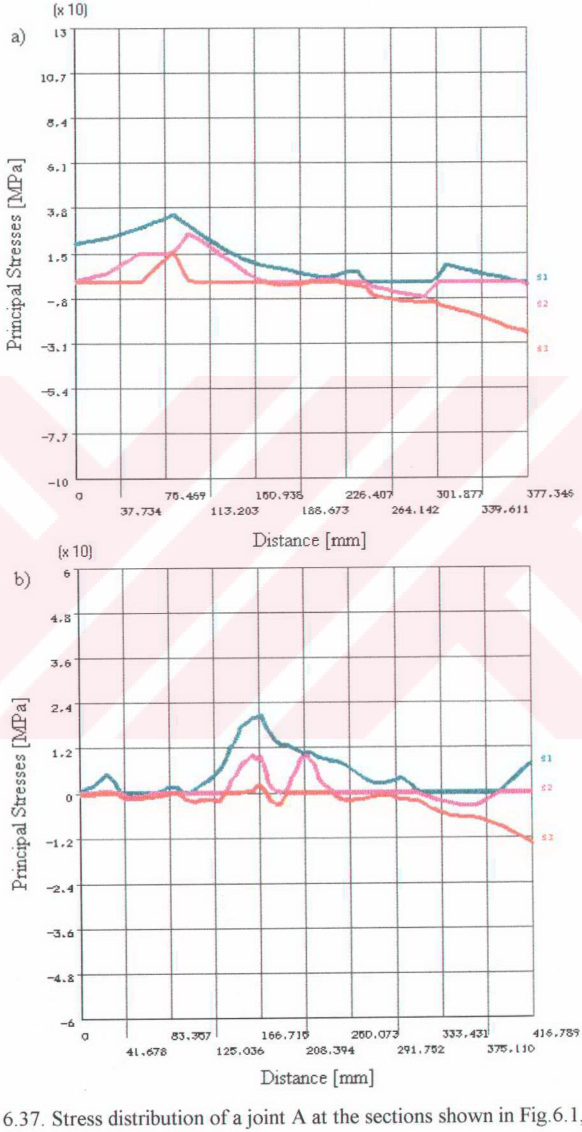

Figure 6.37. Stress distribution of a joint A at the sections shown in Fig.6.1, for the side member thickness =13mm, in road case 1.

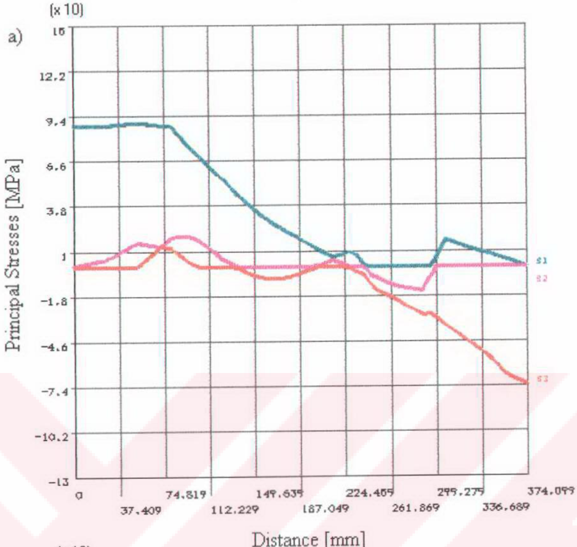

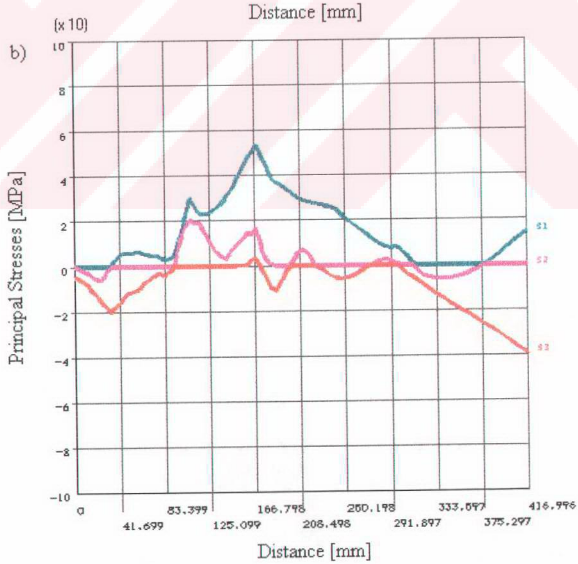

Figure 6.38. Stress distribution of a joint A at the sections shown in Fig.6.1, for the side member thickness =13mm, in road case 3.

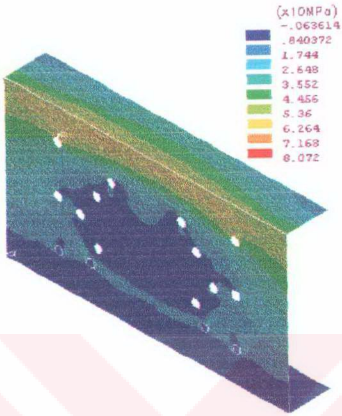

Side member thickness =8mm

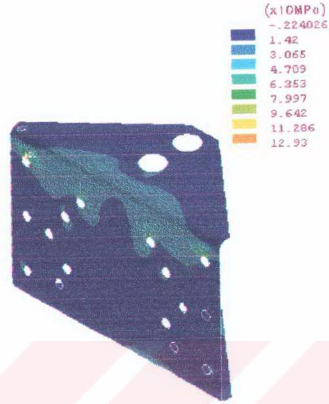

Connection plate thickness t=6mm

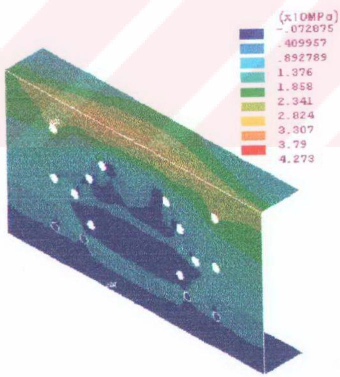

Side member thickness =13mm

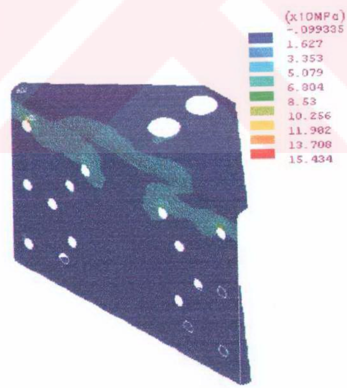

Connection plate thickness t=5mm

Figure 6.39. Maximum principal stress contour on a side member and a connection plate, for road case 1.

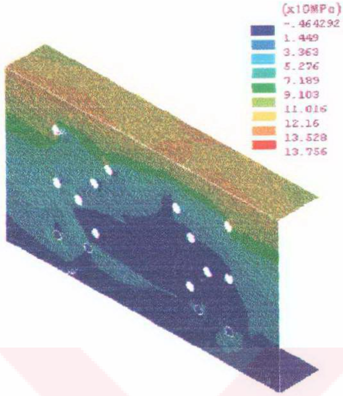

Side member thickness =8mm

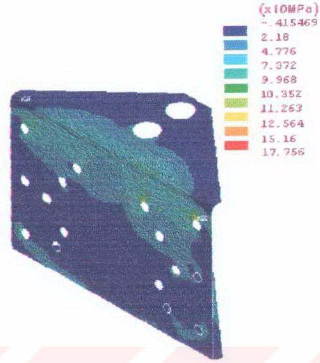

Connection plate thickness t=6mm

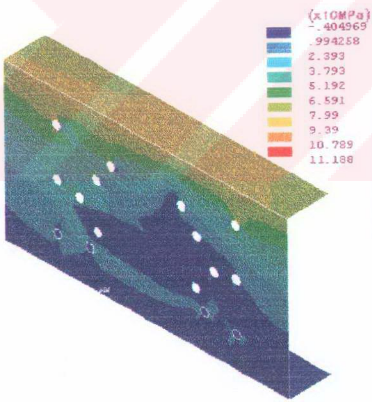

Side member thickness =13mm

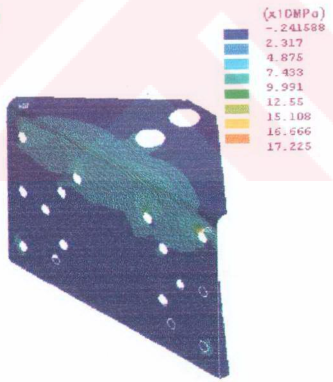

Connection plate thickness t=5mm

Figure 6.40. Maximum principal stress contour a side member and a connection plate, for road case 3.

Figure 6.41 The joint model A2. The rivet locations are changed and connection plate length are decreased.

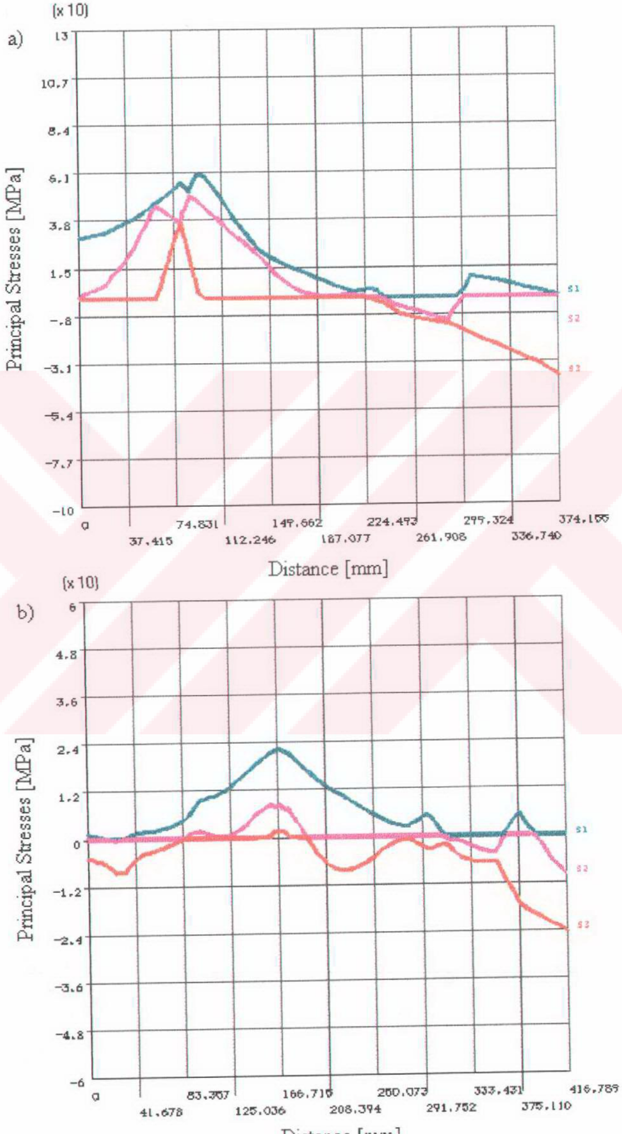

Figure 6.42. Stress distribution of a joint model A2, in road case 1.

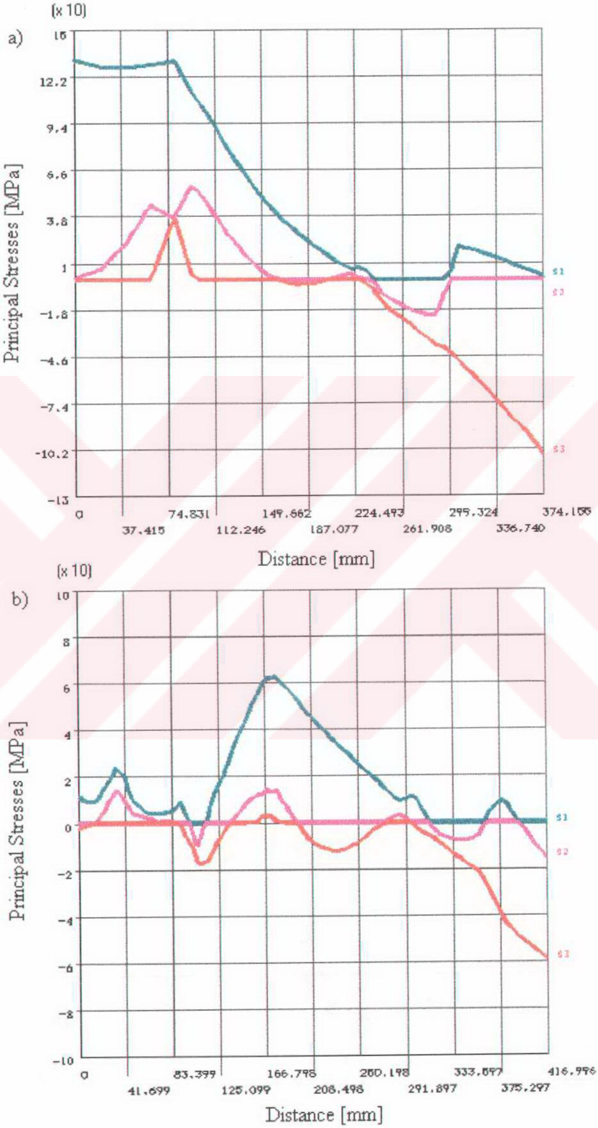

Figure 6.43. Stress distribution of a joint model A2, in road case 3.

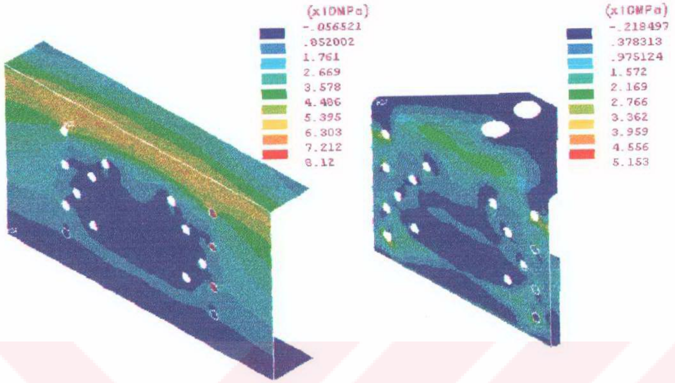

road case 1

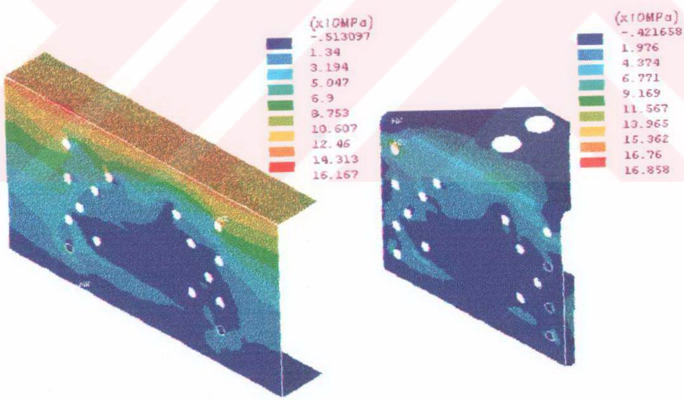

road case 3

Figure 6.44. Maximum principal stress contour on a side member and a connection plate, for joint model A2

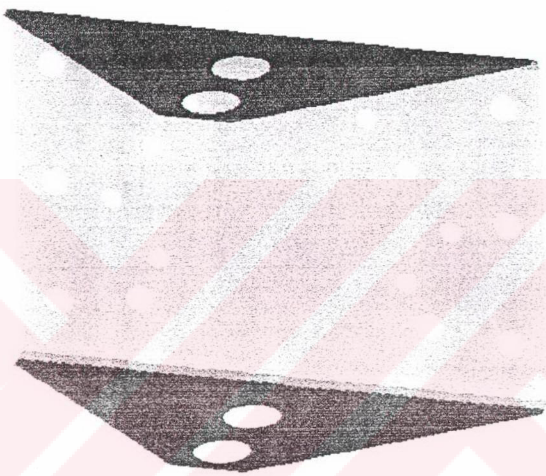

Figure 6.45 Joint model A3. The rivet diameters are increased.

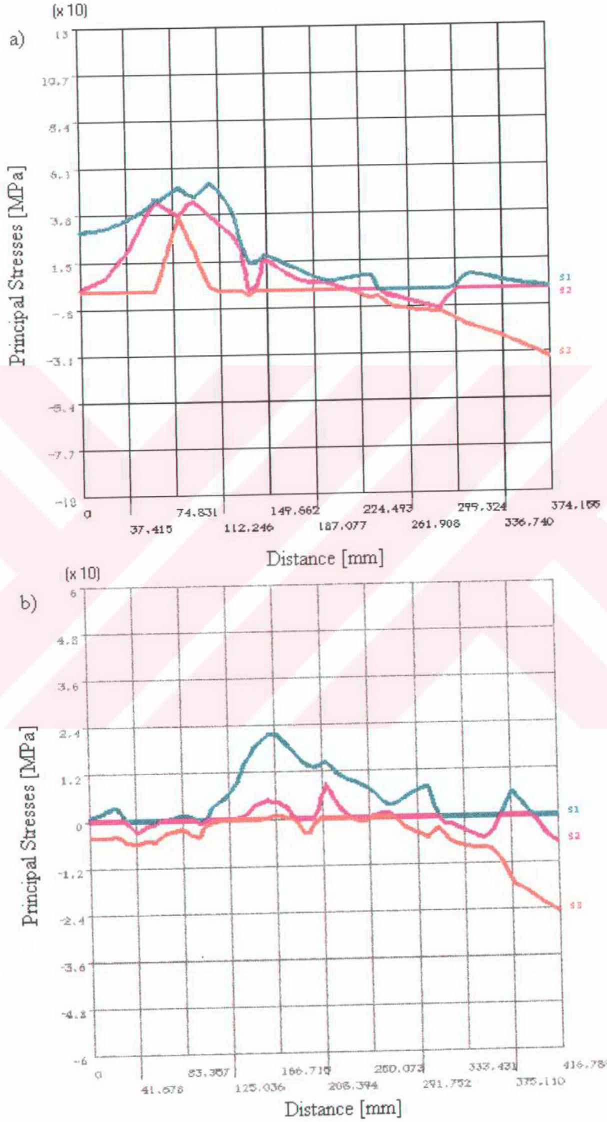

Figure 6.46. Stress distribution of a joint model A3, in road case 1.

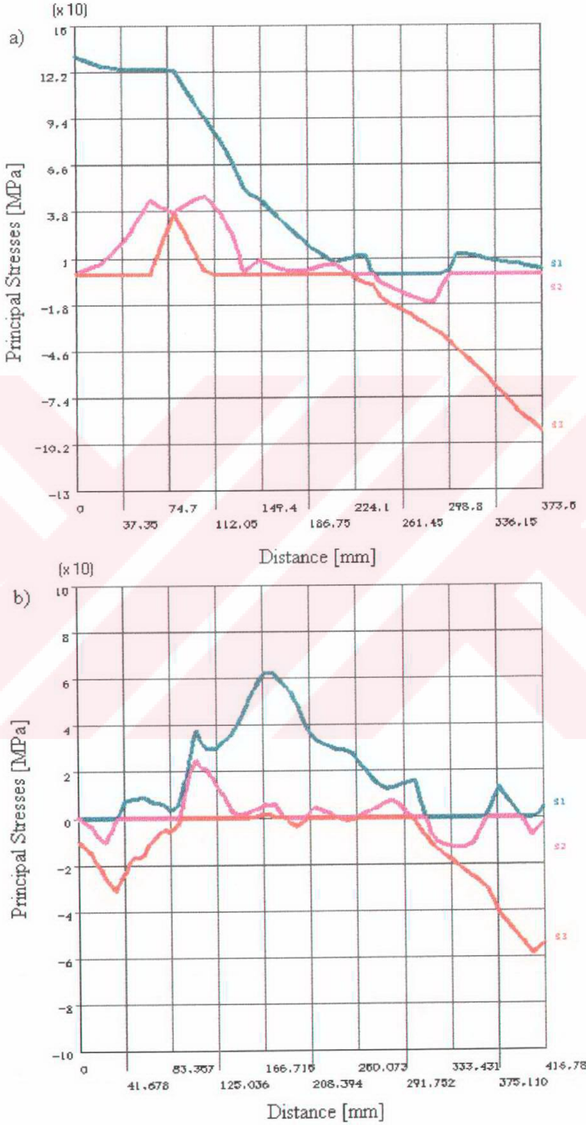

Figure 6.47. Stress distribution of a joint model A3, in road case 3.

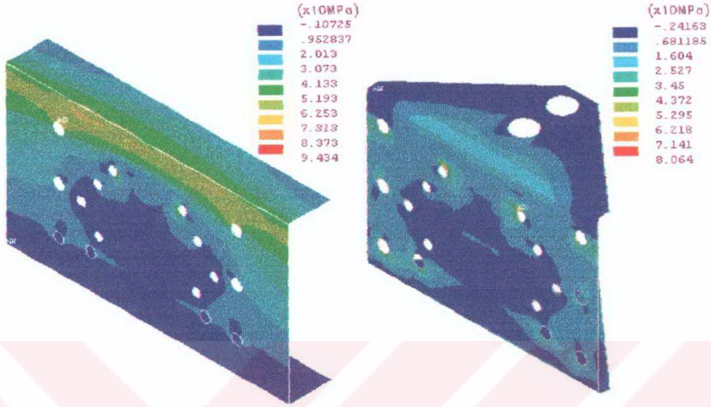

road case 1

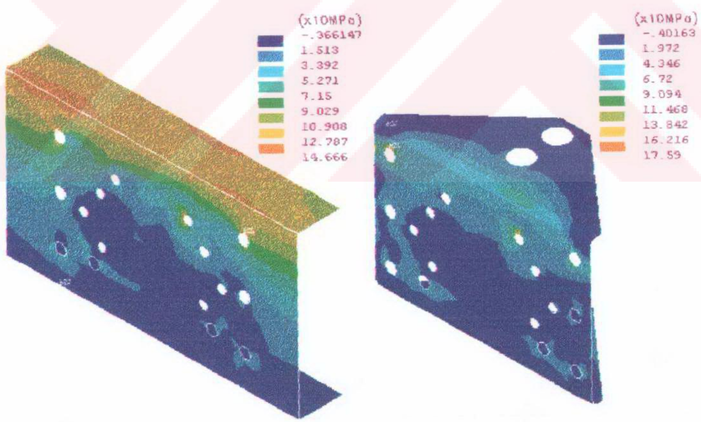

road case 3

Figure 6.48. Maximum principal stress contour on a side member and a connection plate, for joint model A3

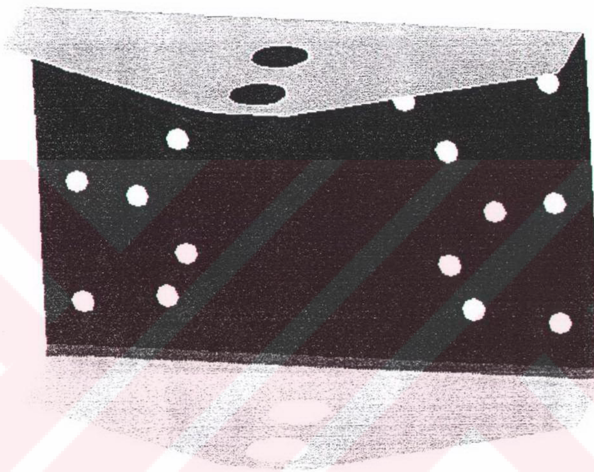

Figure 6.46 Joint model A4 .The connection plate shape are changed.

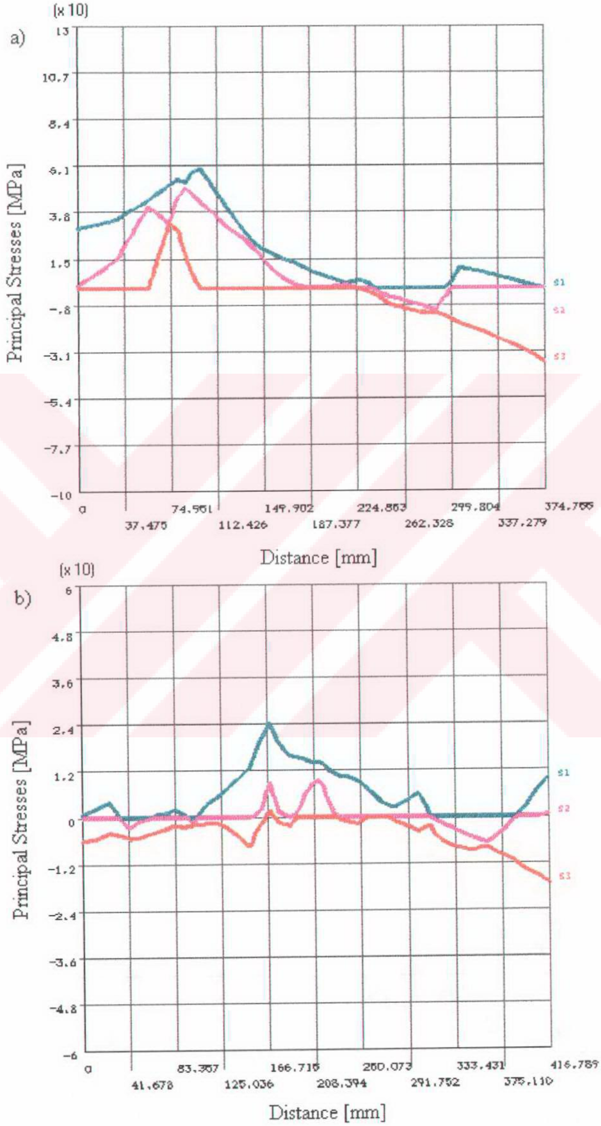

Figure 6.50. Principal stress distribution of a joint model A4, in road case 1.

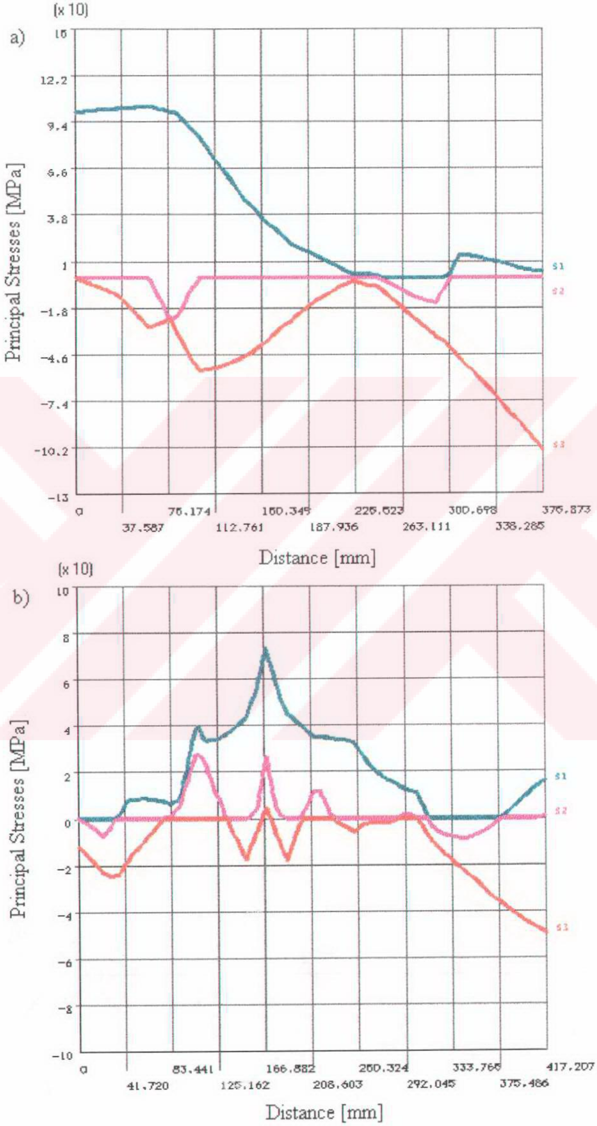

Figure 6.51. Principal stress distribution of a joint model A4, in a road case 3.

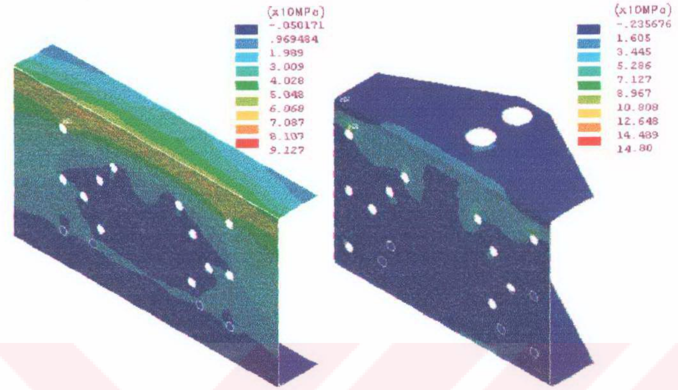

road case 1

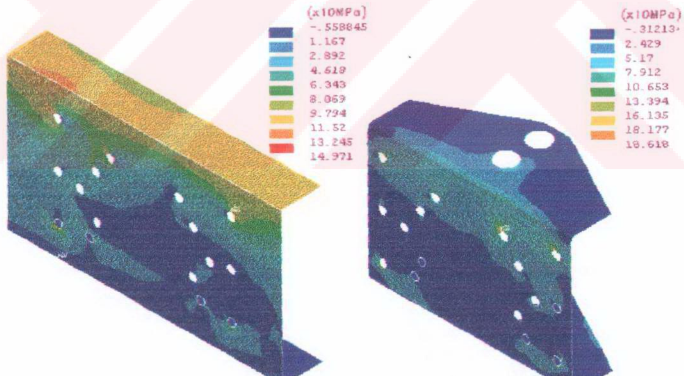

road case 3

Figure 6.52. Maximum principal stress contour on a side member and a connection plate, for joint A4.

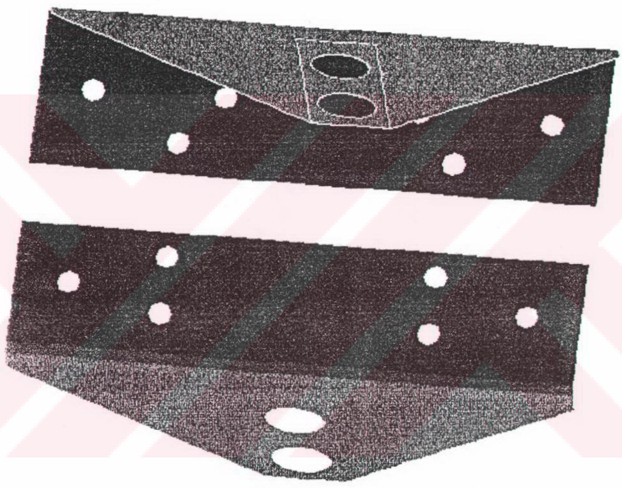

Figure 6.53 The joint model A5. The connection plate model are changed.

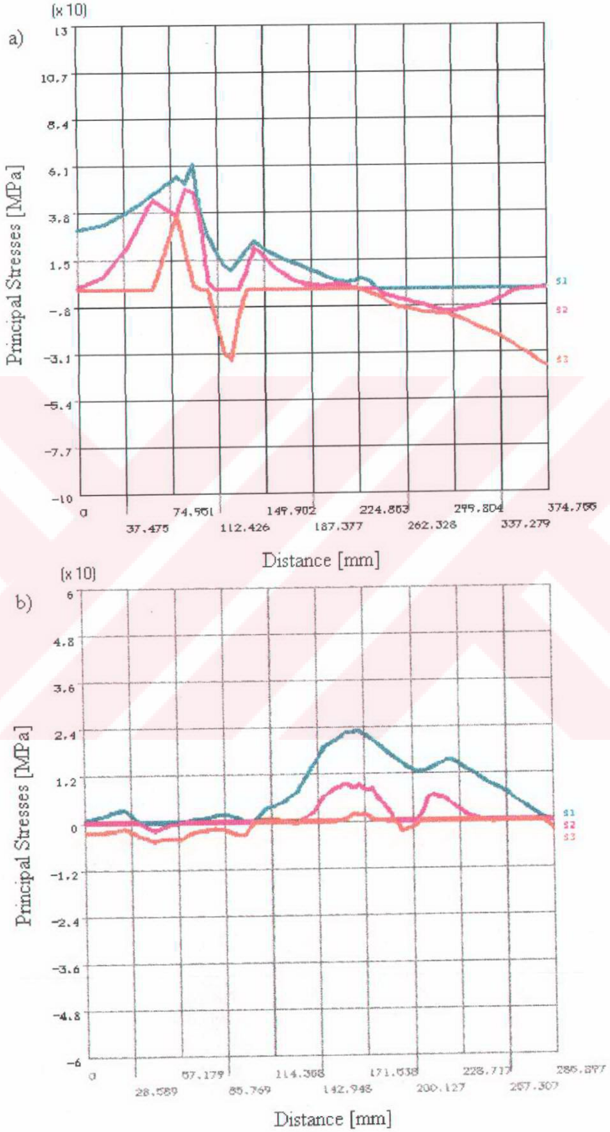

Figure 6.54. Stress distribution of a joint model A5, in road case 1.

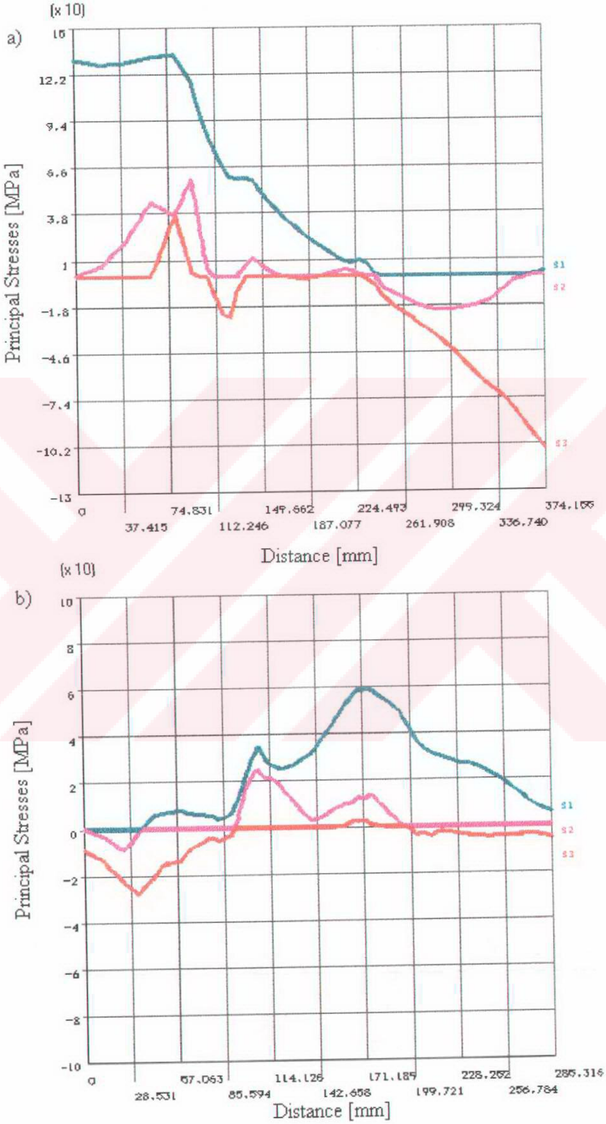

Figure 6.55. Stress distribution of a joint model A5, in road case 3.

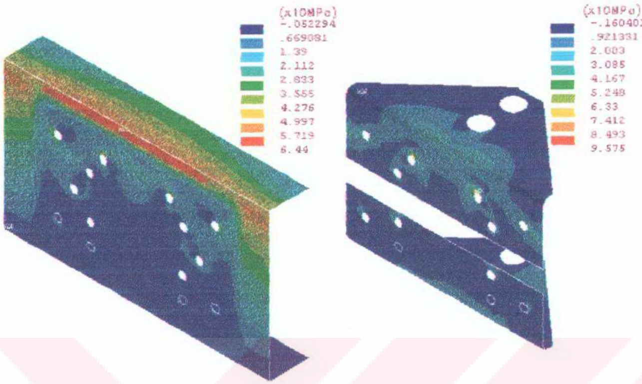

road case 1

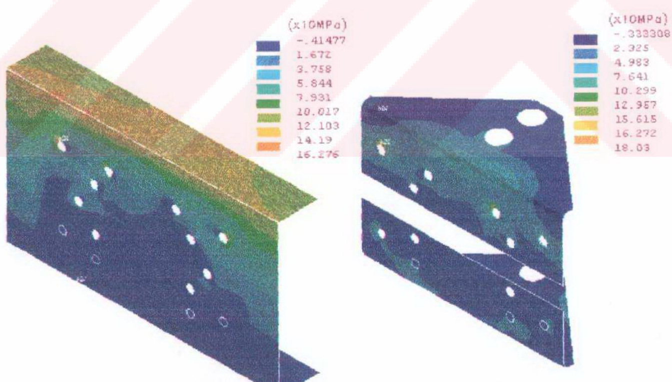

road case 3

Figure 6.56. Maximum principal stress contour on a side member and a connection plate for a joint A5.

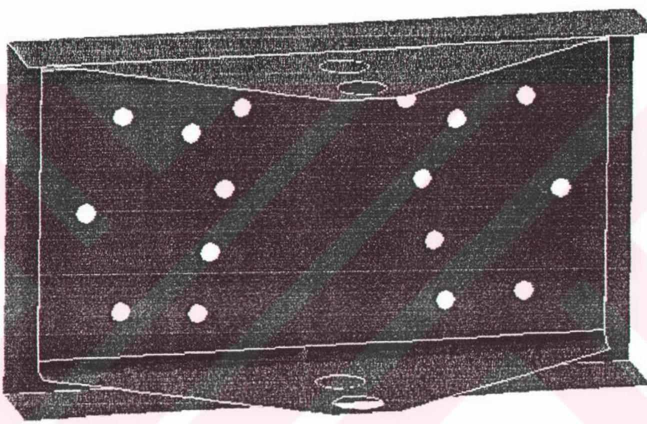

Figure 6.57. Joint model B1 .The rivet location and gusset plate form are changed in joint B

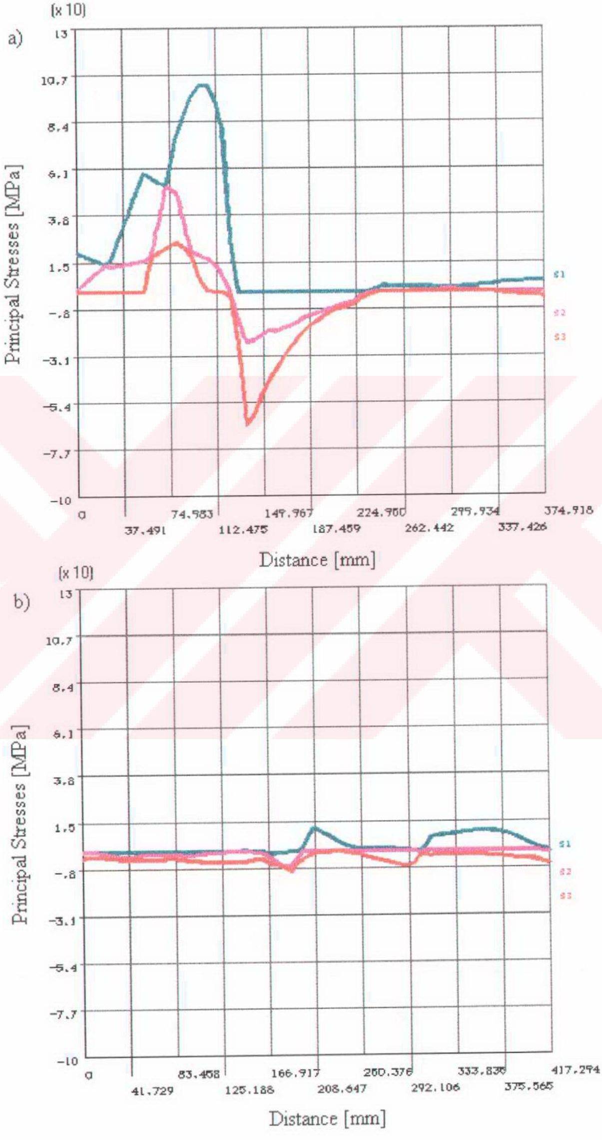

Figure 6.58. Stress distribution of a joint model B1, in road case 1.

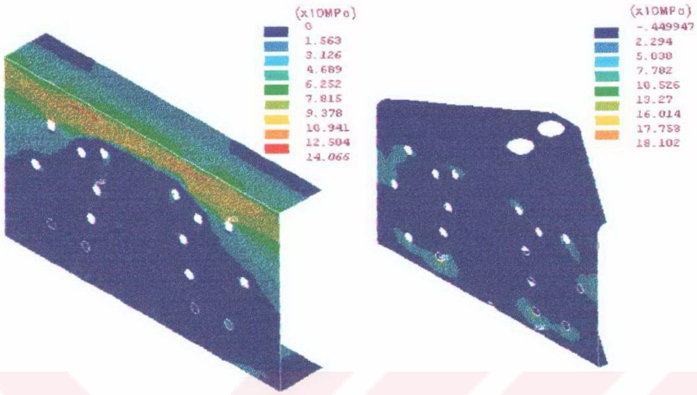

Figure 6.59. Maximum principal stress distribution on a side member and a connection plate, for a joint model B1.

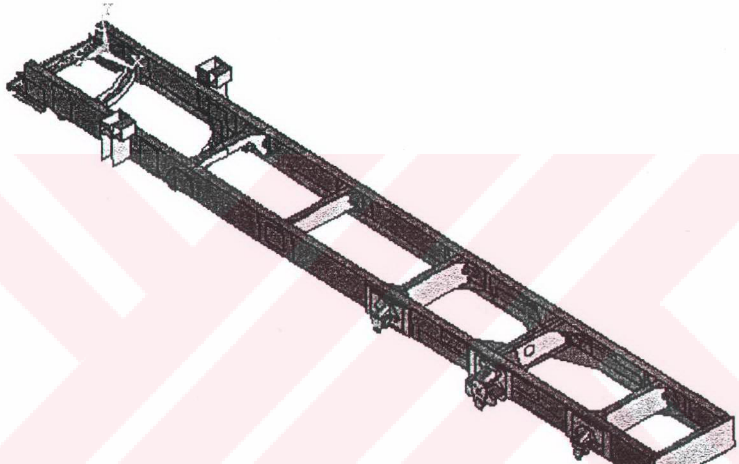

Figure 6.60. Chassis model with different Joints

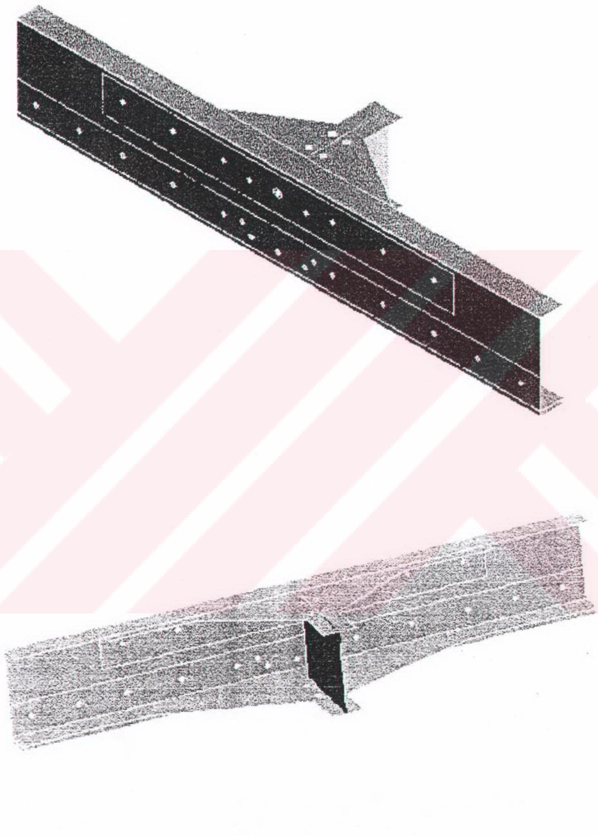

Figure 6.61 Joint model B2

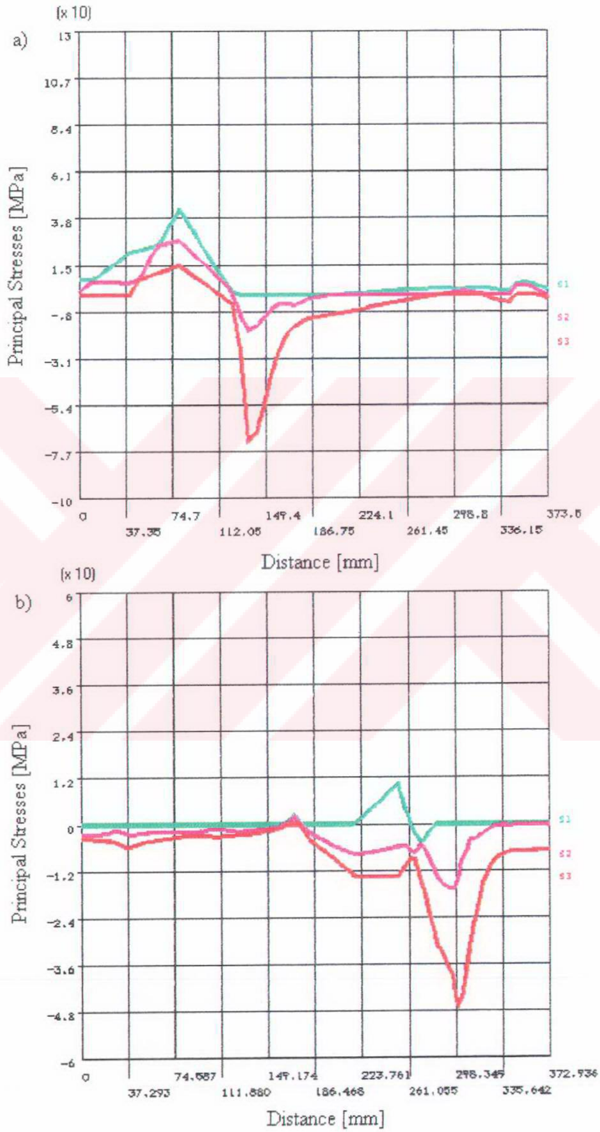

Figure 6.62. Stress distribution of a joint B2, in road case 1.

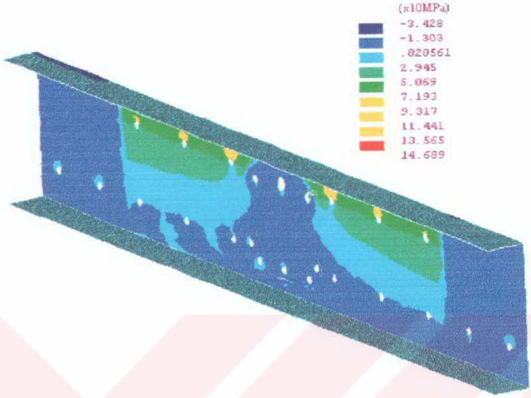

Figure 6.63. Maximum principal stress contour on a side member for a joint B2, in road case 1.

Road case1. It is considered as all the wheels are on a flat surface and the chassis frame is subjected to the vertical bending. The principal stresses obtained from a finite element analysis are shown in Figure from 6.4 to 6.7. The results show that the stress distribution is nearly the same for both model of the chassis. But maximum principal stresses increase sharply across the flanges of the beams for the chassis model (1) which has a rigid spring hanger.

Road case 2. It is considered as one wheel of the rear axle of the truck are free, while the other axles are on a flat surface. Figure 6.8 and 6.9 show the stress distribution of the joint A and B for the chassis model 1. Figure 6.9 and Figure 6.10 show the stress distribution of the joints for the chassis model 2.

Maximum principal stresses occur at the free end of the beam and decrease across to flanges of the beam. The joint B on chassis model(1) is more stressed than the joint B on chassis model (2). The reason is the balance mechanism of the spring hanger in chassis model (2). The load distribution are balanced according to the road condition.

Road case3. It is considered as the one wheel of the front axle is free and the other axle are on a flat surface. Figure 6.11 and Figure 6.12 show the stress distribution of joint A and B for the chassis model l. In both models of the chassis the joint A is most stressed than the joint B.

In order to determine the effect of the joint construction, it has been some changes on joint A .

The thickness of the connection plate is increased up to 10 mm. Figure 6.17 and Figure 6.18 show the stress distribution for a given cross section of joint for the thickness 8mm and 10mm in road case1.When the thickness are increased the maximum principal stress decreases in the connection plate .The reason is that the increasing moment of inertia. But it is important realize that the torsional rigidity increases with the increasing thickness.

The dimension "l " length between the end rivets of the connection plate mountings are decreased. Figure from 6.26 to 6.32 show the stress distribution of a joint for the length l=430mm and l=470mm in road case1 and 3. When the length of the connection plate are increased maximum principal stress decreases in road case 1 and increases in road case 3.

The locations of the rivets are changed shown in Figure 6.33. Figure 6.34 and Figure 6.35 show the stress distribution of a joint in road case1 and case 3.

Thickness of the side member is changed from 8 to 13 mm and the thickness of the connection plate is reduced up to 5mm. When the thickness increases, the maximum principal stress decreases. But the overall weight of the chassis frame increases by %8. Figures 6.39 and Figure 6.40 show the stress distribution for the side member thickness t=13mm.

Figure 6.33 to 6.36 show the results for a new connection plate length (l=350mm) and the changing location of rivets. Maximum principal stress decreases in road case1.

The effect of rivet diameters is shown in Figure from 6.45 to 4.48. When the rivet diameters are increased maximum principal stresses increases.

Figures from 6.49 to 6.56 show the effect of the connection plate shape. Maximum principal stress increases in road case 1 and 3 for a joint A4. Maximum principal stress for joint A5 decreases in road case 1 and increases for road case 3 as shown in Figure 6.56.

The joint B1 shown in Figure 6.57 is a different type of joint B. And the figures from 6.60 to 6.63 is belong to different chassis model. Connection plate consists of two parts. Maximum principal stress distribution along the flange of the side member is smaller compared to stress distribution of joint B in both models of the chassis.

CHAPTER SEVEN
CONCLUSION

The stress distributions of joint A and joint B for the chassis type (1) which has rigid spring hanger and chassis type (2) which has a movable spring hanger has been compared under three different road case.

In road case 1, stress distribution of the joints were nearly the same in both model. But maximum principal stresses across the flanges of the beam increase sharply in chassis model (1) which has rigid spring hanger.

In road case 2, when one of the rear wheel is free; stress distribution of joint B on the chassis model (1) which has rigid spring hanger is larger than the joint B on the chassis model (2) which has movable spring hanger. The reason is that the balance mechanism of the spring hanger on the chassis model(2). So the load distribution are balanced according to the road condition.

In road case 3, when one of the front wheel is free, the joint A more stressed than the joint B for the both model of the chassis frame.

The effect of the constructional change of the joint has been investigated for road case1 and 3. This results can be summarized as follows.

When the thickness of the connection plate are increased the maximum principal stresses decrease because of the increasing moment of inertia

When the length of the connection plate are increased the maximum principal stresses decrease in road case1.

When the rivet diameters are increased maximum principal stresses increase in road case1 and 3.

The flexibility of the joints can be increase by arranging the location of rivets, so maximum principal stresses in the joints are reduced. And the shape of the connection plates also effects the maximum principal stresses.

When the side member thickness is increased 8 to 13mm , the maximum principal stresses decrease. The reason is that the moment of inertia of the side member increases. But it is important realize that the overall weight of the chassis frame increases by up to %8.

Therefore is a substantial change of the side member frame section is not possible, choosing a convenient rivet placement and optimizing connection plate width and thickness seem to be practical solutions for decreasing the stress values.

REFERENCES

ANSYS Procedures(1993), Engineering Analysis System Verification Manual, Swanson Analysis System Inc.,v1, Houston,P.A.,United State of America.

ANSYS Command (1993), Engineering Analysis System Verification Manual, Swanson Analysis System Inc.,v2, Houston,P.A.,United State of America.

ANSYS Elements (1993), Engineering Analysis System Verification Manual, Swanson Analysis System Inc.,v3, Houston,P.A.,United State of America.

ANSYS Theory (1993), Engineering Analysis System Verification Manual, Swanson Analysis System Inc.,v4, Houston,P.A.,United State of America.

Barsoum, R.S. & Gallagher, R.H. (1970). Finite Element Analysis of Torsional and Torsional-Flexural Stability Problems. International Journal of Numerical Methods in Engineering, v 2, n 3, pp335-352.

Bathe, K.J. (1982). Finite Element Procedures in Engineering Analysis. Prentice Hall Inc. Englewood Cliffs, New Jersey.

Bathe,K.,J. and Wiener,P.M.(1983). On elastic plastic analysis of I beams in bending and torsion. Computers structures, v117,n5-6,pp711-718.

Beerman, H. J. (1989). The Analysis of Commercial Vehicle Structures, St Edmundsbury Press Limited, Bury St Edmunds, Suffolk.

Beerman, H. J. (1977). Warping inhibition in the joints of vehicle frames with open cross-section members. Leichtbau der Verkehrsfahrzeuge,pp1-6.

Beerman, H. J. (1980). Torsion of commercial vehicle frames with open and closed cross section members. Automobiltechnische Zeitschrift (ATZ),N9,pp 459-464.

Beerman, H. J.(1984). Static analysis of commercial vehicle frames. Int.J.Vehicle Design, v5,pp 26-52.

Chandrupatla, T.R. & Belegundu, A. (1991). Introduction to Finite Elements in Engineering. Prentice Hall. Inc., Englewood Cliffs, New Jersey.

Chee, K., Faris, G.A., (1992). Finite element method for buckling analysis of plate structures. Journal of Structural Engineering, v.119, n.4,pp1048-1067.

Chin,C.K., Al-Bermani, F.G. & Kitipornchai, S. (1992). Stability of Thin-Walled Members Having Arbitrary Flange Shape and Flexible Web. Engineering Structures, v 14, n 2, pp. 121-132.

Ereke, M. (1989). Şasi ve karoseriyi zorlayan kuvvetler ve boyutlandırma ilkeleri. Mühendis ve Makina, c 30, n 353.

Ereke, M. (1989). Yaklaşım metodu yardımıyla kamyon şasisinde burulma açısı ve burulma katılığının hesabı. Mühendis ve Makina, c 30, n 355.

Ereke, M. (1989). Açık profill kesitli şasi çerçevesinde kesit çarpılmasının burulma rijitliği bakımından önemi. Mühendis ve Makina ,c30, s 357.

Ereke, M. (1996). Torsional static analysis of commercial vehicle frames considering joint flexibility. Bulletin of the Technical University of Istanbul.

Graves-Smith, T.R. & Sridharan, S. (1978). A finite strip method for the buckling of plate structures under arbitrary loading. Int. J. Mech. Sci., v 2, n 10, pp685-693.

Johnson, C.P. & Will, K.M. (1974). Beam buckling by finite element procedure. J. Struct. Div., ASCE, v 100, n 3, pp669-685.

Kwangju L., Nikolaidis, E. (1992). Identification of flexible joints in vehicle structures. AIAA Journal, v.30, n.2,pp 482-489.

Megson, T.H.G.and Alade,G.A.(1976). Structural analysis of ladder frames under torsion. The Inst.of Mech.Eng.Proc.,v90,38/76

Mohr,G.A.(1992). Finite elements for solids, fluids, and optimization. Oxford University Press,Inc.,NewYork.

Nath B.(1974). Fundamentals of finite elements for engineers. The Athlone Press of the University of London 1974.

Oehlschlaeger,H.(1977). Considering cross-member orifices in the structural analysis of commercial vehicle frames. Leichtbau der Verkehrafahrzeuge,4.

Oehlschlaeger, H. (1977). Influence of the nodal design on the torsional stiffness and torsional stresses of torsionally flexible frames of commercial vehicles. Automobile Industrie, n2 ,s69.

Oehlschlaeger, H. (1980). Einflauβ der Knotenauslegung auf Verdrehsteife und-beanspruchungen von verwindungsweichen Nutzfahrzeugrahmen. Automobile Industrie. 2/80,69-76.

Pries,H., Wille, H.C. (1984). Some examples of modern vehicle design analysis by finite element method. Int.J.of Vehicle Design ,v5,n1/2,pp53-66.

Tidbury, G. H.. (1980).Vehicle structural analysis. Introductional Journal of Vehicle Design, v 1,n 2,pp165-166.

Yun, C.B. & Shinozuka, M. (1980). Identification of nonlinear structural dynamic systems. Journal of Structural Mechanics, v8, n.2, pp 187-203.

Zienkiewicz, O.C. (1985). The Finite element Method. Mc Graw Hill Company,UK.

APPENDIX A
THE COMPUTER PROGRAM

A1.INTRODUCTION

ANSYS program is a general-purpose computer program for finite element analysis that was used in the solution. The ANSYS program has many finite element capabilities ranging from a simple linear, static analysis to a complex , nonlinear, transient dynamic analysis.

A typical ANSYS analysis has three distinct steps:

- Build the model
- Apply loads and obtain the solution
- Review the results

A2. BUILD THE MODEL

Building a finite element model requires more of an ANSYS user's time than any part of the analysis. First a jobname is specified then, PREP7 preprocessor is used to define the element types, element real constants, material properties and the model geometry.

A2.1. Defining Element Type

The ANSYS program element library contains over 100 types element. It may be that are span beam, plane, volume, shell, axisymmetric etc. implies the discipline (structural ,thermal, magnetic etc.), the characteristic shape of the element (line, quadrilateral, brick etc.), and the whether the element lies in 2-D space or 3-D space.

A2.2 Defining Element Real Constants

Element real constants are properties that are specific to a given element type, such as cross-sectional properties of a beam element.

A2.3. Defining Material Properties

Most element types require material properties that depending on the application, material properties may be linear, nonlinear, and/or anisotropic.

A2.4.Creating the Model Geometry and Meshing

Once you have defined material properties, the next step in analysis is to create the finite element model geometry. There are two methods to create the finite element model : Solid model and direct element model generation.

A3. APPLY LOADS AND OBTAIN THE SOLUTION

This step is to define analysis type and analysis option apply loads, and boundary conditions.

A3.1. Apply Loads

Loads in the ANSYS program are divided into six categories. DOF Constraints, Forces, Surface Loads, Body Loads, Inertia Loads , Caupled Field Loads.

A4.REVIEW THE RESULTS

Once the solution has been calculated, ANSYS postprocessor can be used to review the results.

APPENDIX B
SUBMODELING

B1.1 INTRODUCTION

Submodeling is a finite element technique used to get more accurate results in a region of your model. Often in finite element analysis, the finite element mesh may be too coarse to produce satisfactory results in a region of interest, such as a stress concentration region in a stress analysis. The results away from this region however may be adequate.

To obtain more accurate results in such region, there are two options:

a) reanalyze the entire model with grater mesh refinement
b) generate an independent, more finely meshed model of only the region of interest and analyze it.

Obviously, option (a) can be time consuming and costly (depending on the size of the overall model). Option (b) is the submodeling technique.

Submodeling is also known as the cut-boundary displacement method or specified boundary displacement method. The cut boundary is the boundary of the submodel which represents a cut through the coarse model. Displacements calculated on the cut boundary of the coarse model are specified as boundary conditions for the submodel.

Submodeling is based on St.Venant's principle, which states that if an actual distribution of forces is replaced by a statically equivalent system, the distribution of stress and strain is altered only near the regions of load application. This implies that stress concentration effects are localized around the concentration; therefore, if the boundaries of the submodel are far enough away from the stress concentration, reasonably accurate results can be calculated in the submodel.

A side from the obvious benefit of giving more accurate results in a region of model, the submodeling technique has other advantages.

* It reduces, or even eliminates, the need for complicated transition regions in solid finite element models.
* It enables to experiment with different designs for the region of interest (different fillet radii, for example)
* It helps in demonstrating the adequacy of mesh refinements.

B1.2 HOW TO DO SUBMODELING

1. Create and analyze the coarse model.
2. Create the submodel.
3. Perform cut boundary interpolation.
4. Analyze the submodel.
5. Verify that the distance between the cut boundaries and stress concentration is adequate.